Modelling soil – vegetation – atmospheric interactions of radon products in a Belgian Scots pine forest site

Jordi Vives i Batlle (✉)

Belgian Nuclear Research Centre (SCK•CEN), Boeretang 200, 2400 Mol, Belgium
Tel: +32 (0)14 33 88 05
Fax: +32 (0)14 32 10 56
e-mail: jordi.vives.i.batlle@sckcen.be

This is a preprint of an article in the Journal of Environmental Radioactivity (DOI: https://doi.org/10.1016/j.jenvrad.2024.107607)

Abstract

A soil-vegetation-atmospheric transfer (SVAT) model for radon and its progeny is presented to improve process-level understanding of the role of forests in taking-up radionuclides from soil radon outgassing. A dynamic system of differential equations couples soil, tree (Scots pine) and atmospheric processes, treating the trees as sources, sinks and conduits between the atmosphere and the soil. The model's compartments include a dual-layer soil column undergoing hydrological and solute transport, the tree system (comprising roots, wood, litter, and foliage) and the atmosphere, with physical processes governing the transfers of water and radon products between these compartments. A dose post-processor calculates dose rates to the trees from internal, external, and surface radiation exposures. The parameterisation is based on measurement data from the Grote Nete Valley in the Belgian Campine region.

The model suggests that the tree intake of radon progeny is principally from the atmosphere, whereas radium is mainly taken-up from soil by the root uptake process, leading to an additional fraction of ingrown radon progeny in the tree by this route. It is also suggested that atmospheric uptake of radon is an essential mechanism when evaluating the tree uptake of ^{214}Po, ^{214}Pb and ^{218}Po and subsequent decay products. The model also indicates a slow uptake of radionuclides by the tree roots, with timescales in the order of years, leading to different dose rates for young and mature trees. The importance of foliar surface deposition, leading to a dominance of surface doses to the tree needles, is also highlighted. These mechanisms, ignored in most assessment models, are necessary improvements for assessment tools dealing with the impact of radon and its progeny in forests, with regard to legacy sites with ^{226}Ra contamination.

Key words: Radon; SVAT model; forests; radionuclide cycling; RadoNorm

1. Introduction

The objective of radioecological modelling of forests is to mathematically simulate the distribution, cycling and sinks of radionuclides in vegetation considered together with the surrounding soil and atmosphere. There is a dual purpose to this type of modelling: research and impact assessment. The research model aims at understanding the role of trees as 'biological pumps' cycling radionuclides and water by mathematically representing the key processes in an integrated way. This is achieved by implementing the governing equations of processes controlling the movement of water (e.g. evapotranspiration, groundwater flow, sap flow) and energy (e.g. solar irradiation, changes in temperature), and linking the radionuclide transport to these fluxes (Diener et al., 2017). The impact assessment model focusses on making an estimation of the radiation doses to man and the environment (Calmon et al., 2009). Both types of models require prediction of radionuclide transfer dynamics within forest compartments, running in parallel with water transport (Rantavaara et al., 2001).

Radionuclide exchange in forests combines multiple complex processes involving soil water and element transport, root uptake (Li et al., 2001), sap flow (Hölttä et al., 2006), the biological pumping function of trees, or transpiration (Monteith and Unsworth, 2007), translocation between parts of the tree (Van den Hoof and Thiry, 2012), immobilisation and storage, washout and litterfall (Berg, 2000; Copplestone et al., 2000), all of which regulate the entry, circulation, storage and exit of substances in the tree. This requires understanding the biogeochemical cycling of the elements in the forest (Raven et al., 2001), taking account of seasonal variations in soil hydrology (Perez-Sanchez et al., 2012), modelling water movement from a shallow water table to the root zone (Raes and Deproost, 2003; Vincke and Thiry, 2008), considering the translocation of substances inside the tree (Ceulemans et al., 2003; Van den Hoof and Thiry, 2012) and understanding the behaviour of radionuclides in soil and vegetation (Casadesus et al., 2008). It is necessary to consider radon-specific processes such as soil exhalation, atmospheric aerosol formation and plant deposition (Porstendörfer, 1994; Vives i Batlle et al., 2011). One must face-up to this complexity and achieve a fit-for-purpose model that is sufficiently complex to be realistic, but sufficiently simple to be practical.

The present study, developed within the EC RADONORM project (https://www.radonorm.eu/), aims to cover the gap between research and assessment modelling, by providing a realistic way to capture the main processes but making the necessary simplifications to reduce the number of parameters required, to be a viable model for use in assessments. The emphasis is on treating the trees as an integral part of the soil plant–atmosphere continuum, acting as sources, sinks and conduits between the atmosphere and the soil and effectively linking these terrestrial realms in a soil–plant–atmosphere continuum. Such a model can provide an integrated context to field studies in radium-contaminated sites (Sweeck et al., 2024; Vanhoudt et al., 2021), as part of site characterisation studies for remediation.

Following atmospheric deposition, the primary source of tree contamination is direct interception of aerosol by the canopy, followed by further translocation from foliar surfaces to structural components of the tree. After the initial exposure period, the dominant process is the recycling caused by the self-cleaning of the canopy by precipitation wash-off (throughfall) and litterfall (which returns radionuclides to soil after decomposition) as well as re-entry by root uptake of the radionuclides that have migrated into the soil profile (Diener et al., 2017).

When the contamination is located below ground, the transfer processes from soil to tree are most important, including vertical migration in the soil column, root uptake, vertical transport, and the recycling of radionuclides from trunk to leaves and back to soil by the litterfall. The balance between input from below the tree and the return processes to the ground can take a long time to achieve (Vincke and Thiry, 2008), with daily oscillations caused by changes in evapotranspiration and

seasonal oscillations caused by fluctuations in the water table between wet and dry periods. The number of processes involved and associated uncertainties require simplification of the problem during modelling, with fine adjustments to the model to achieve a water balance between the volumetric water content of the soil column layers, the net recharge, surface water inflow/outflow, evaporation from soil and transpiration from the tree.

The objective of this paper is to prove the feasibility of a fit-for-purpose, simplified modelling approach to solve the SVAT problem for radon and its progeny, using approximations to the hydrology, vegetation and atmospheric processes requiring less parameters than used in more complex solute transport, geochemical and vegetation models e.g. Hydrus (Šimůnek et al., 2006) and PHREEQC (Deckmyn et al., 2008; Parkhurst, 1995). The resulting prototype model is applicable to situations in which the source of contamination is both below ground (the ^{226}Ra and associated progeny in the soil) and above-ground (the atmospheric aerosol of radon progeny that arises from radon emanated and exhalated from the ^{226}Ra in the soil).

Radon gas (^{222}Rn) and its decay products (collectively described as "radon") are not only an issue in houses but also in the outdoor environment where it escapes from the soil and enters the environment, which can be an issue for biota on the surface. For modelling purposes, one can assume that the radon progeny forms small particle clusters (unattached fraction) which in turn attach to aerosol particles (attached fraction). Both the unattached and attached fractions have a given deposition velocity (Chamberlain, 1991; Porstendörfer, 1994; Porstendörfer et al., 1978; Vives i Batlle et al., 2011), so that the radon progeny can be taken up by trees, whence they can return to the forest surface by litterfall (Fig. 1).

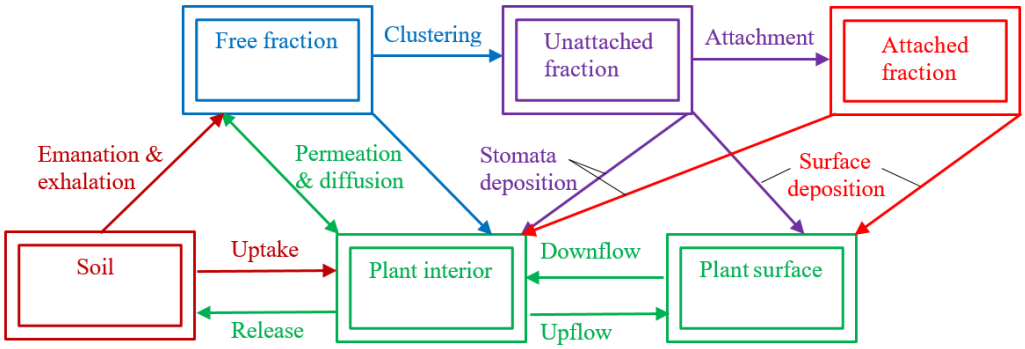

Figure 1: Processes influencing uptake of turnover of soil-emanated radon by vegetation.

Radon progeny deposited onto trees can contribute significantly to the plant dose, justifying their modelling in context of a SVAT system. It is reasonable to assume that the presence of trees can have an impact on the atmospheric distribution of the radon, potentially effecting changes in the balance between the unattached and the attached fractions. By considering four basic processes: diffusion through stomata without aspiration, permeation through plant leaves, direct deposition of particles and translocation, a model can reproduce basic characteristics of the airborne radon mixture (i.e. the proportions of the different aerosol components) and assess in a holistic way the impact of radon in both vegetation and its surrounding environment.

1.1 Study hypotheses

In this study, a soil-vegetation-atmospheric transfer (SVAT) model for radon and its progeny was built by coupling the atmospheric radon model by Vives i Batlle et al. (2011) with the SCK CEN ECOFOR (ECOlogical model for FOrest Radioecology) SVAT model developed and documented in the previous EC TERRITORIES project (Brown et al., 2019; Diener et al., 2017; Urso et al., 2019). At the start of our investigation, we aimed to use this integrated model to evaluate four hypotheses:

a) That the uptake of radon progeny by the tree roots occurs at a slow timescale (of the order of decades) compared with atmospheric uptake, such that the soil-tree transfer ratios take decades to stabilise.
b) That tree uptake of the aerosol of radon progeny is a significant contribution to the total plant activity compared with root uptake, so that this mechanism should not be ignored in impact assessment.
c) That the activity deposited on the foliage surfaces results in a significant component of the total dose received by the tree, representing a third component in addition to external and internal exposure.
d) That forest vegetation can induce a disequilibrium in the atmospheric aerosol of the radon progeny, with potential implications for site remediation.

2. Model design

The model includes the following compartments: (a) a dual-layer soil column undergoing hydrological and solute transport, (b) the tree system (comprising roots, wood, litter, and foliage) and (c) the atmosphere (free, unattached, and attached aerosol fractions), as shown in Fig. 2.

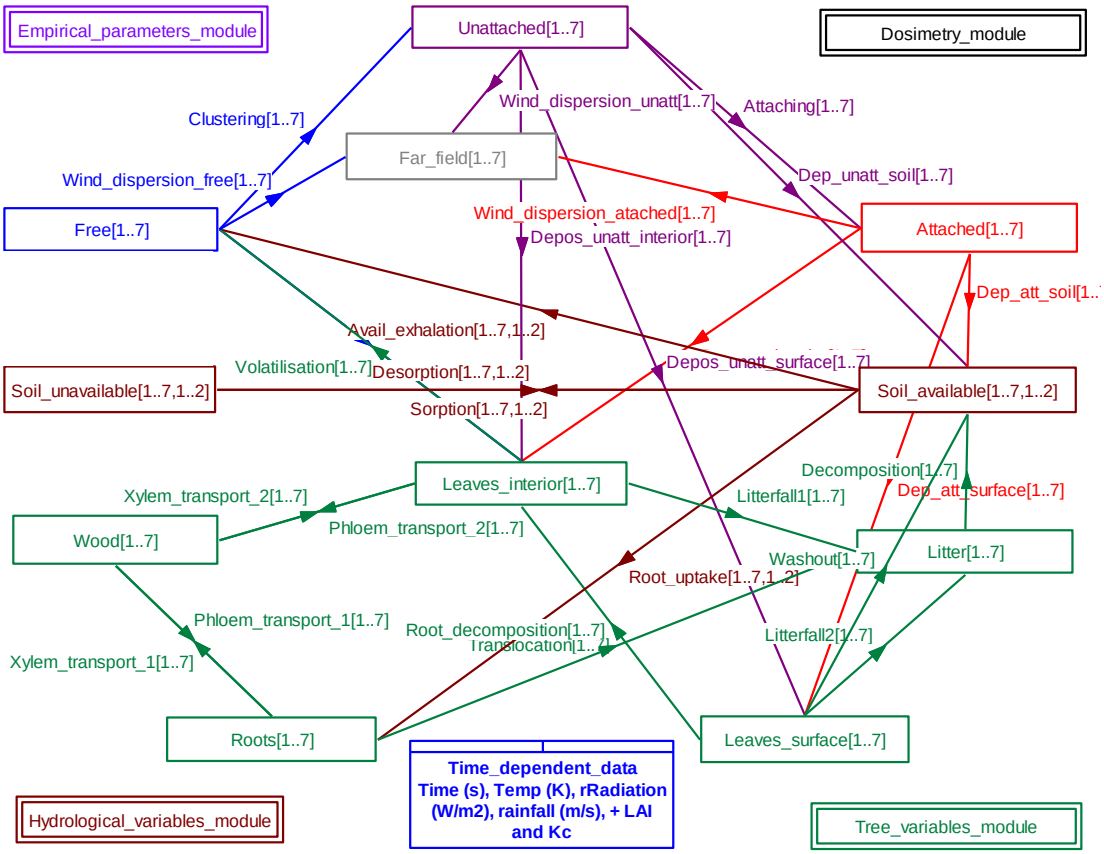

Figure 2: Model schematic with components indexed according to substance (1 to 7, with 1 corresponding to water and > 1 to radionuclide) and soil layer (1 to 2).

The key processes considered are soil transport (infiltration, Darcy flow, capillarity, retardation, diffusion, and soil gas exhalation), transfer to vegetation (wet and dry deposition, root uptake, xylem/phloem transport and evapotranspiration), wind dispersion and return of radionuclides to soil (litterfall and decomposition). A dose post-processor calculates radiation doses to the trees and the non-human biota living in the forest floor.

The model was parameterised using a combination of data from the Grote Nete Valley in the Belgian Campine region (Sweeck et al., 2024) with some supplementary pine tree physiology data from the nearby Kepkensberg radioecological observatory site in the Belgian Campine region (Vanhoudt, 2015).

2.1 Soil submodel description

The soil submodel is a substantially simplified interpretation of processes that, in their full version, would require solving the Richards' equation for transport of water across the soil column (Richards, 1931), coupled with the transport (advection and dispersion) equation for the solutes (Diener et al., 2017). In this sense, it can be best described as being semi-mechanistic. Although not exactly "simple," our approach is not as complex, parametrically demanding and computationally expensive as the fully mechanistic approach. It is adequate to predict the time-dependent radionuclide concentration in conditions of moderate flow rate, due to its use of Darcy law. If the flow approaches zero or high flow occurs (e.g. in high hydraulic conductivity soils with fractures), flow linearity is lost, and our approximation may lose applicability.

We used a "tipping-bucket" type of approach whereby up and down flows of water in the two soil layers are regulated by saturation, field capacity and residual water switches. The depth of the upper soil is assumed to be 0.24 m, based on our own observations of the depth of the organic layer at a Belgian Campine forest site. The depth of the lower soil is taken as 1.5 m, chosen to encompass the entirety of the pine tree root system, which we estimated to be 1.4 m. Each soil layer has two sub-compartments S_{ij}^{u} and S_{ij}^{a} (unavailable and available - *aka* soil solution - fractions, respectively). These compartments are given here in matrix notation with indices i = 1 to 7 for water and the radionuclides ^{226}Ra, ^{222}Rn, ^{218}Po, ^{214}Pb, ^{214}Bi and ^{214}Po, respectively, and j = 1 to 2 for surface and subsurface soil layers. The equation for the available fraction is as follows:

$$\frac{dS_{ij}^{a}}{dt} = \begin{cases} (In_i R_{i1} + \emptyset_{i2}^{u} K_2^{FC} + W_i + Dc_i) K_1^{sat} - \emptyset_{i1}^{d} K_1^{FC} - (Ru_{i1} + Ev_{i1}) K_1^{res} + Dp_i^{un} + Dp_i^{att} - Ex_{i1}^{a} - Srp_{i1} + Des_{i1} + d_{i1}^{soil} \\ (for\ j = 1) \\ (\emptyset_{i1}^{d} K_1^{FC} + Dc_i) K_2^{sat} - (\emptyset_{i2}^{u} + \emptyset_{i2}^{d}) K_2^{FC} - (Ru_{i2} + Ev_{i2}) K_2^{res} - Ex_{i2}^{a} - Srp_{i2} + Des_{i2} + d_{i2}^{soil} \\ (for\ j = 2) \end{cases}$$

And, for the unavailable fraction:

$$\frac{dS_{ij}^{u}}{dt} = \begin{cases} 0\ (for\ i = 1) \\ Sorp_{2j} - Des_{2j} - \lambda_2 S_{2j}^{u}\ (for\ i = 2) \\ Sorp_{ij} - Des_{ij} + \lambda_{i-1} S_{i-1j}^{u} - \lambda_i S_{ij}^{u}\ (for\ i > 2) \end{cases}$$

The volumetric water content for all layers is continuously updated by the model based on the component fluxes defined as follows:

- In_i is the input flux for water and radionuclides from precipitation.
- R_{ij} is the retardation factor (see equation definition below).
- $\emptyset_{ij}^{u}$ and $\emptyset_{ij}^{d}$ are the soil water upflow and downflow fluxes.
- W_i is the washout of water from tree foliage, controlled by the foliage washout coefficient.
- Dc_i is the plant root decomposition.
- Ru_{ij} and Ev_{ij} are the fluxes for water root uptake and evaporation from soil (see vegetation model description).
- K_i^{sat} is a saturation switch: $K_i^{sat} = \begin{cases} 0 \text{ if } \theta_i > \theta_i^{max} \\ 1 \text{ by default} \end{cases}$, where θ is the volumetric water content.

- K_i^{FC} is a field capacity switch: $K_i^{FC} = \begin{cases} 0 \text{ if } \theta_i \leq f_i^{FC} \\ 1 \text{ by default} \end{cases}$, where f is the field capacity.
- K_i^{res} is a residual water switch: $K_i^{res} = \begin{cases} 0 \text{ if } \theta_i \leq \theta_i^{res} \\ 1 \text{ by default} \end{cases}$, where θ^{res} is the residual water capacity.
- Dp_i^{un} and Dp_i^{att} are the deposition fluxes for the unattached and attached fraction of the radon progeny aerosol.
- Ex_{ij}^{a} is the radon exhalation flux from the soil available fraction.
- Srp_{ij} and Des_{ij} are the sorption and desorption rates between the soil unavailable and available fractions. For radon gas, an arbitrarily high desorption rate is used. The desorption rate for radon progeny is functionally linked to the sorption rate such that the equilibrium rate of radionuclide concentrations in two compartments is equal to the K_d.
- d_{ij}^{soil} is the radioactive decay: $d_{ij}^{soil} = \begin{cases} 0 \text{ for } i = 1 \\ -\lambda_i S_{ij}^a \text{ for } i = 2 \\ \lambda_{i-1} S_{i-1,j}^a - \lambda_i S_{ij}^a \text{ for i} > 2 \end{cases}$

At the top of the first layer, water and solutes enter by infiltration - an input rate governed by the precipitation (Baes and Sharp, 1983). When the soil column is fully saturated with water, infiltration is stopped, and the excess is diverted to runoff.

Downward flow in porous soil is approximated by Darcy's law in a homogeneously permeable medium without gravity (horizontal column of length L), given by $Q = -\frac{kS_A}{\mu L}\Delta p$ where Q is the flow, S_A is the surface area, L is the column length, k is the permeability, μ is the dynamic viscosity and Δp = $p_b - p_a$ is the pressure difference applied (Pa). Implicit in this expression is the acceleration of gravity, according to the expression $\Delta p = \rho g \Delta h$. We assume here conditions of free drainage, given that, for the case study considered, the soil considered is sandy soil with a low water table (much below the 1 – 1.5 m of depth of the root zone), and we assume no extremes of soil dryness or saturation. For the hydraulic conductivity, we assume an empirical exponential parameterisation for the hydraulic conductivity: $H_i = H_i^S e^{-\alpha\left(\frac{\theta_{si}-\theta_i}{\theta_{si}-\theta_{di}}\right)}$, where θ_{si} and θ_{di} are the saturated and dry soil moisture contents and H_i^S is the saturated hydraulic conductivity (Kendy et al., 2003).

The water up-flow through the soil column can only be approximately calculated. As a starting point, we used Newton's dynamic equation for a viscous non-compressible liquid, assuming Poiseuille flow. We deduced an approximate equation for the total volume $V = Nv$ for the volumetric rate in the soil pores as $\frac{dv}{dt} = \frac{1}{2\tau}\varepsilon S_A s^2 \left(\frac{\varepsilon S_A}{2V} - \frac{1}{4}\rho g \eta \left(\frac{s}{\gamma}\right)^2\right)$ where ε is the porosity, S_A is the surface area of the soil compartment (a nominal value of 1 m^2 can be used, as S_A cancels out when converting the equation to a rate $\frac{1}{v}\frac{dv}{dt}$), ρ is the density, η is the viscosity, s Is the sorptivity constant, γ is the surface tension and τ is a correction factor to compensate for the fact that soil water does not ascend linearly, but in a tortuous part. This flow is only possible for positive values of this equation.

Element transport is linked to soil water via retardation processes in soil (with link to the K_d of the element, assumed to be dependent on soil moisture), with the retardation equation $R_{ij}^f = \left(1 + \frac{\rho_i^b (1-\varepsilon_i) K d_j}{\theta_i}\right)^{-1}$, where ρ_i^b is the bulk density of the soil layer i, ε_i is the porosity, Kd_j is the soil – water distribution coefficient of the radionuclide j, and θ_i is the volumetric water content.

The model also assumes a reversible interaction between the exchangeable (soil solution) and fixed (soil matrix) fractions of radionuclides present in the soil, according to first-order exchange kinetics.

The last key element of the soil model is the exhalation rate for radon gas, produced in the soil by the decay of existing ^{226}Ra and released via the available fraction. The soil radon exhalation flux depends on the exhalation rate $r_{ij}^{ex,a}$, modulated by soil moisture according to: $Ex_{ij}^{a} = \frac{r_{ij}^{ex,a}}{d_i}\left(1 - \frac{\theta_j}{\theta s_j}\right)$ to take into account the reduction of air channels in the soil as saturation increases. The exhalation rate is calculated using the diffusive modelling approach of UNSCEAR (1993) as $Ex_{ij}^{a} = C_s^{Rn,a} E \sqrt{\frac{D_c \lambda_{Rn}}{\varepsilon}}$. This approach does not include the effects of tortuosity or atmospheric pumping in surface soil layers. Here, $C_s^{Rn,a}$ is the concentration of radon in the soil (assumed in secular equilibrium with the parent ^{226}Ra), E is the soil emanation coefficient, D_c is the diffusion coefficient, λ_{Rn} is the decay constant of radon, ε is the porosity and d_i is the depth of the soil layer. It is noteworthy that at equilibrium, this approach leads to a radon concentration in air $C_a^{Rn} = \frac{C_s^{Rn,a} E \rho_{bulk} \sqrt{\frac{D_C \lambda_{Rn}}{\epsilon}}}{v_w + \lambda_{Rn} h_{eff}}$ where ρ_{bulk}, v_w and h_{eff} are the soil bulk density, the wind speed and the radon vertical dimension of mixing; that is, the relevant height to derive volume for the local atmosphere. This equation provides a way to validate the model with atmospheric radon concentration measurements, which was done successfully in this study.

The model assumes that radon exhalation occurs from the soil available fraction, because any radon generated in the unavailable fraction is immediately transferred to the available fraction, by virtue of the large desorption rate used. We ignore the fact that the radon emitted by the bottom layer has to pass through the top layer to reach the atmosphere, with a resulting reduction of the flux, because (a) the diffusion length of radon is higher than the thickness of the top layer, (b) the top layer has a lower volumetric water content, leaving abundant pore space for radon gas to diffuse and (c) upper soil has significantly lower density than bottom soil; hence the approximation holds true in this context.

Lastly, decay chains are included using the Bateman equations based on the radioactive decay half-life of the radionuclides involved (Bateman, 1910).

2.2 Atmospheric submodel description

The atmospheric fractions of radon and its progeny are represented by three compartments: free, unattached, and attached). Each sub-model contains compartments for the decay chain of radon: ^{222}Rn $\Rightarrow$ ^{218}Po $\Rightarrow$ ^{214}Pb $\Rightarrow$ ^{214}Bi $\Rightarrow$ ^{214}Po. The α-disintegrations ^{218}Po $\Rightarrow$ ^{218}At and ^{214}Bi $\Rightarrow$ ^{210}Tl are neglected due to their low intensity. In addition, there is a sink compartment to represent wind dispersal of the airborne material to the far field with a rate constant equal to $r = v_w h_{eff}$.

Wet deposition of radon and its progeny is not explicitly considered. This arises from a balance between model complexity and practicality, as the scavenging of differently-sized fractions of a rapidly dispersing aerosol is difficult to model. This decision is based on four reasons: (a) the low solubility of ^{222}Rn in water (Lerman, 1979), (b) the fact that dry deposition is a more continuous process, with rainfall occurring a small fraction of the total time, (c) during rainfall, soil exhalation reduces due to soil waterlogging, depleting the pool of aerosol particles available for precipitation and (d) the plant-intercepted fraction strongly decreases with rainfall, at least for moderate to intense events, due to water and particle dripping (Gonze et al., 2014). Nevertheless, the model still uses rainfall-driven infiltration to calculate the water balance in the soil.

Full details on the radon aerosol modelling are given in a previous publication (Vives i Batlle et al., 2011). The starting point is the formation of products of the radon decay exhaled from the soil in the form of "free atoms." After formation, they react very quickly (in less than a second) with vapours and gases, forming an airborne mixture of free atoms and clusters or colloids of "free radon progeny." The latter tend to attach to atmospheric particles (Porstendörfer, 1994). This is represented in our model by linear transfer rates. The model then calculates the deposition of the unattached and attached

fractions of the airborne radon progeny, as well as diffusion of radon gas from the free fraction to the vegetation.

The deposition flux ϕ (in m^{-2} s^{-1}) as a function of the initial activity concentration of Rn in air C_a^{Rn} is calculated as $\varphi = \frac{C_a^{Rn} v_d}{\lambda_{Rn}}$, where λ_{Rn} is the decay constant for radon and v_d is the deposition velocity. The product φS_A (where S_A is the surface area) is the rate constant for the process. Surface deposition is the most important parameter for removal of radon progeny from air (Porstendörfer, 1994), with a rate of removal $\frac{v_d S_A}{V_G}$where S_A and V_G are the surface area available for interception and the volume of gas above it, respectively.

Different fractions of radon progeny (e.g., gas, unattached and attached fractions) show different deposition fluxes. The calculation is influenced by the equilibrium factor $F = \frac{0.105C(^{218}Po)+0.516C(^{214}Pb)+0.379C(^{214}Bi)+6\times10^{-8}C(^{214}Po)}{C(^{222}Rn)}$, expressed in terms of the activity concentrations of the progeny and their potential alpha energy concentration (El-Hussein, 1996; Porstendörfer, 1994). The calculation also depends on the fraction of the unattached progeny, f_p, which can be calculated as $f_p = \frac{0.105C_{unat}(^{218}Po)+0.516C_{unat}(^{214}Pb)+0.379C_{unat}(^{214}Bi)+6\times10^{-8}C_{unat}(^{214}Po)}{C(^{222}Rn)\times F}$.

The atmospheric model calculates F and f_p in real time. It can be assumed that all the attached progeny have the same deposition velocity v_{att}, and the contribution of the attached progeny to the total surface deposited activity can be ignored due to their much lower deposition velocity (Schmidt and Hamel, 2001).

The deposition velocity is calculated using the equation $v_d(z) = \frac{kv_f}{ln(kv_f zD^{-1})}$ (Tadmor, 1973) where $1/z$ is the surface per unit volume ratio of the air column, k is von Karman's constant = 0.4 (USEPA, 2004), v_f is the friction velocity and D is the molecular diffusivity (i.e. the diffusion coefficient), relating to particles of a given size z, i.e. unattached versus attached fractions. A consequence of the above equation is that v_d onto surfaces having a high surface area per unit volume ratio, such as leafy plant systems, is significantly higher than onto flat ground (Ferrandino and Aylor, 1985). Therefore, the leaf area index, λ_L, is an important parameter for our model.

We used average deposition velocities for the unattached and attached fractions onto ground, $v_d^A$and v_d^U, from a previous study (Porstendörfer, 1994), and it can be seen that $v_d^U \gg v_d^A$ and that both increase with the surface area of the vegetation. We devised a simple method to scale the deposition velocity as an exponential function of λ_L, taking advantage of the fact that there is a reasonable good exponential fit for the data, leading to the following scaling relationships: $v_d^{unat} = \alpha_U e^{\beta_U \lambda_L}$, and $v_d^{att} = \alpha_A e^{\beta_A \lambda_L}$. The rate constant for deposition r_d is easily derived as $r_d = v_d \times SV^{-1} = \frac{v_d}{h}$, where SV^{-1} is the surface area per unit volume of the air column of height h above the plant (Chamberlain, 1991).

2.3 Vegetation submodel description

The vegetation sub-model contains 5 compartments: Roots, Wood, Litter, and foliage, divided into surface and interior. The Root uptake and evapotranspiration processes have already been described in the description of the soil model.

The root uptake is calculated by an exponential root water uptake model (Li et al., 1999), assuming an exponentially decreasing root density distribution with depth z: $RD(z) = RD_0\left[1 - \frac{1}{1+e^{-Ez}} + \frac{1}{2}e^{-Ez}\right]$, where RD_0 is the root density at z = 0 and E is an empirical 'extinction coefficient'. Provision is made for waterlogging (anaerobiosis, using a water stress coefficient).

Both root uptake and the plant transpiration rate are controlled by the evapotranspiration demand, the main engine for water and solutes transport in the tree. This is modelled by the Monteith equation (Monteith and Unsworth, 2007), which calculates ET_o, the reference evapotranspiration, namely the volume of water per unit area and time, as $ET_0 = \frac{\Delta(R_n - G) + \frac{\rho_a c_p (\delta e)}{r_{av}}}{\lambda_v \rho_w \left[\Delta + \gamma\left(1 + \frac{r_s}{r_{av}}\right)\right]}$. In this equation, Δ is the rate of change of saturation specific humidity with air temperature, Rn is the net solar radiation flux , *G* is the sensible heat flux into the soil, ρ_a is the dry air density, c_p is the specific heat capacity of air, δe is the vapour pressure deficit, r_{av} is the resistance of air (atmospheric conductance), γ is the psychrometric constant, r_s is the resistance of tree foliage stoma (surface or stomatal resistance), λv is the latent heat of water and ρ_w is the density of water. The model calculates the actual evapotranspiration as a function of ET_0 by scaling by the actual water content of the plant compartment.

Fluids are assumed to circulate through the plant upwards (xylem upflow governed by the Poiseuille equation) and downwards (phloem downflow along an osmotic pressure gradient for a 20% sucrose solution) (Saupe, 2009) allowing translocation of the radionuclides with these flows.

The ascending transport of water through the tree vessels (xylem flow rate) is calculated by means of the Poiseuille equation. The pressure differential above gravity necessary to maintain a certain velocity *v* is $\Delta\Psi_p = \frac{8\eta h v}{r^2}$. The rate constant is the flow divided by the surface area and the height of the tree (dimensions of d^{-1}), or $r = \frac{1}{8\eta}\left(\frac{r}{h}\right)^2 \Delta\Psi_p$.

The descending flow rate (phloem flow rate) is calculated by an approximate equation, derived by us. The starting point is the Poiseuille equation, but now the pressure gradient is a downward osmotic pressure: $\Psi_{osm} = \frac{\pi r^4}{8\eta h} iMRT$, where we have used the Morse equation for the osmotic pressure (Amiji and Sandmann, 2002), expressed as $\Pi = iMRT$. Here, *i* is the dimensionless van 't Hoff factor for sugars in water, the solute is assumed to be sucrose ($C_{12}H_{22}O_{11}$) (Zimmermann and Ziegler, 1975), which makes up around 20% of sap (Saupe, 2009), *T* is the absolute temperature, *R* is the ideal gas constant, r is the vessels' radius, *M* the molarity of the solution, η the viscosity and h the tree height. The molarity of the sap can be calculated as $\frac{\rho}{M_a}\left(\frac{f}{1-f}\right)$ where ρ is the density of the sucrose and *f* is the fraction of solute (sucrose) by mass; hence an expression for the descent rate of the phloem is $v = \chi \frac{i\rho r^2 RT}{8\eta h M_a}\left(\frac{f}{1-f}\right)$, where an additional phloem drag coefficient to account for the tortuosity of the vessels.

Water interception by the canopy, washout, absorption, and leaching are considered as transfer factors and litterfall plus litterfall decomposition are modelled by an empirically derived linear transfer rate. The model incorporates a simple logistic model for stand density, quantifying the effect of tree density on the leaf area index and, therefore, on water availability to the trees.

Just as element transport is linked to soil water via retardation processes in soil (with a link to the K_d of the element, assumed to be dependent on soil moisture), in the vegetation model, empirically-derived selectivity coefficients (Gielen, 2013; Gielen et al., 2016) link element fluxes to the water fluxes in plants in an approach similar to the BioRUR model (Casadesus et al., 2008).

The interaction of atmospheric radon with plant foliage follows four processes: (a) ^{222}Rn diffusion through stomata and ^{222}Rn permeation through plant epidermis (free fraction to plant interior); (b) ^{218}Po, ^{214}Pb, ^{214}Bi and ^{214}Po interception by stomata (unattached and attached fractions to plant interior); (c) ^{218}Po, ^{214}Pb, ^{214}Bi and ^{214}Po deposition (unattached and attached fractions to plant surfaces); and (d) Transfer of deposited ^{218}Po, ^{214}Pb, ^{214}Bi and ^{214}Po from plant surface to plant interior.

The plant interception of unattached and attached fractions derives from the number of particles lost per unit time from the air column is $\frac{dN_D}{dt} = -\left(\frac{n_S \sigma_S \lambda_L v_d}{h}\right) N_D$, where n_S is the number of plant stomata per unit plant interception area, σ_S is the surface area of the individual stomata, N_D is the number of atoms of radon progeny in an air column of surface S_G and h is the radon vertical dimension of mixing. This gives a rate constant of $r_{dep(stomata)} = \frac{n_S \sigma_S \lambda v_d}{h}$.

The foliage stomata radius ρ_{st} was assumed to vary between a minimum value of zero and a maximum value ρ_{max} as stomata open and close within a daily cycle of 8.63×10^5 s: $\rho_{st} = \rho_{max}\left[1 - int\left(\frac{t}{43200}\right) + 2\, int\left(\frac{t}{86400}\right)\right]$. This discontinuous equation can slow down considerably the Runge-Kutta numerical solver used by *ModelMaker*. This was resolved by changing the default integration method to Gear's method (Gear, 1971), which is more appropriate for stiff systems. For long duration model runs where sub-daily variation is not required, execution can be accelerated by taking: $\rho_{st} = \frac{1}{2}\rho_{max}$.

Diffusion of radon gas through stomata was represented by the diffusion equation $-\frac{dN}{dt} = \frac{DA}{l_s}(c_{out} - c_{in})$ where $\frac{dN}{dt}$is the number of atoms passing through the membrane per unit time (m^{-2} s^{-1}); A is the area of the leaf that is acting as a conduit, i.e. the stomata, relating to the surface area of soil S_A through the equation $A = \lambda_L S_A n_s \sigma_s$. Here, D is the diffusion coefficient D, l_s is the length of the stomatal channel; and $c_{out} - c_{in}$ is the difference in radon concentration between outside air and the substomatal cavity.

If $C_{out} > C_{in}$, radon diffuses into the leaf according to $c_{out} - c_{in} = \frac{N_{Rn}^{out}}{hS_A} - \frac{N_{Rn}^{in}}{\lambda_L L \gamma S_A}$. The plant is assumed to have a porosity γ, with a thin epidermis compared with the overall thickness of the leaf, L. An upper limit of $LS_A\lambda_L$ for plant leaves can thus be calculated. Hence, $-\left.\frac{dN_{Rn}^{out}}{dt}\right|_{diff} = \left.\frac{dN_{Rn}^{in}}{dt}\right|_{diff} = \lambda_L \frac{D}{l_s} S_A n_s \sigma_s \left[\frac{N_{Rn}^{out}}{hS_A} - \frac{N_{Rn}^{in}}{\lambda_L L \gamma S_A}\right] = \frac{\lambda_L D n_s \sigma_s}{h l_s} N_{Rn}^{out} - \frac{D n_s \sigma_s}{L \gamma l_s} N_{Rn}^{in} \equiv r_{in}^{diff} N_{Rn}^{out} - r_{out}^{diff} N_{Rn}^{in}$, whereupon the rate constants for the process are $r_{in}^{diff} = \frac{\lambda_L D n_s \sigma_s}{h l_s}$ and $r_{out}^{diff} = \frac{D n_s \sigma_s}{L \gamma l_s}$.

The permeation of free fraction through foliage can be interpreted as transport through a membrane that is acting as a resistance to diffusion: $\frac{dN}{dt} = \frac{-KS}{w}(c_{in} - c_{out})$, where N is the number of atoms of parent radon in the atmospheric compartment (free progeny > 5 orders of magnitude below can be neglected); K is the permeability of the membrane (m^2 s^{-1}); S is the cross-sectional area of the flow (m^2), equal to the total surface of the leaf minus the surface area of the stomata, $\lambda_L S_A(1 - n_s \sigma_s)$; w is the thickness of the membrane, equal to the thickness of the leaf's epidermis; and c_{in}-c_{out} is the concentration gradient between outside and inside the leaf.

Substitution of these equations yields $-\left.\frac{dN_{Rn}^{out}}{dt}\right|_{perm} = \left.\frac{dN_{Rn}^{in}}{dt}\right|_{perm} = \frac{K\lambda_L(1 - n_s\sigma_s)}{l_s}\left(\frac{N_{Rn}^{out}}{h} - \frac{N_{Rn}^{in}}{\lambda_L L \gamma}\right) \equiv r_{in}^{perm} N_{Rn}^{out} - r_{out}^{perm} N_{Rn}^{in}$, from where the rate constants are $r_{in}^{perm} = \frac{K\lambda_L(1 - n_s\sigma_s)}{h l_s}$ and $r_{out}^{perm} = \frac{K(1 - n_s\sigma_s)}{L\gamma l_s}$. During the day, the flow through the plant membrane can be neglected because the proportion of stomata area $n_s\sigma_S$ is as high as 15%. However, during the night, diffusion through the barrier will be the only route of entry into the leaf and therefore this process cannot be neglected.

For ease of model construction, we derived a single expression for a semi-permeable leaf:
$-\frac{dN_{Rn}^{out}}{dt}\Big|_{dgas} = \frac{dN_{Rn}^{in}}{dt}\Big|_{gas} = \left(Dn_s\sigma_s + K(1-n_s\sigma_s)\right)\left[\frac{\lambda_L}{hl_s}N_{Rn}^{out} - \frac{1}{L\gamma l_s}N_{Rn}^{in}\right] \equiv r_{in}^{gas}N_{Rn}^{out} - r_{out}^{gas}N_{Rn}^{in}$

As material is washed-out from plant leaves, it can become partially sequestered by the stomata (translocation). The total open surface area of the leaf (sum of the aperture area of all stomata) with respect to plant surface area is $n_s\sigma_S$. Hence, the translocation rate of washed-out particles back into the plant is $r_{trans} = r_W n_s \sigma_S$ and the leaf leaching-out rate should be $r_{leach} = r_W(1 - n_s\sigma_S)$, adding to the total washout rate r_W.

2.4 Dosimetry sub-model description

The dosimetry part of the model is based on dose coefficients extracted from the ERICA Tool (Version 2). In this version, the internal dose rate calculations are simplified so the low energy (< 10 keV) β, the higher energy β + γ and the α components of the dose can be directly aggregated into a single internal dose coefficient. However, radiation weighting factors can be introduced if desired.

For external exposure, we consider that the tree is above ground, given the emphasis placed on irradiation from atmospheric radon and the progeny. These changes are consistent with ICRP Publication 136 (ICRP, 2017).

Activity concentrations for radionuclide *i* (i.e. ^{226}Ra, ^{222}Rn, ^{218}Po, ^{214}Pb, ^{214}Bi and ^{214}Po) in each model compartment *j*, were calculated as $a_{ij}^{soil} = \frac{A_{ij}}{M_j} = \frac{N_{ij}\lambda_i}{\rho_j d_j S_A}$ (soil), $a_{ij}^{plant} = \frac{N_{ij}\lambda_i}{f_j M_j}$ (plant matter) and $a_{ij}^{air} = \frac{A_{ij}}{V} = \frac{N_{ij}\lambda_i}{hS_A}$. The model uses these activity concentrations to calculate unweighted absorbed doses, using the following equations:

- External dose rates from radionuclide *i* in the atmosphere for the attached, unattached and free fractions are calculated as $DR_{i,fraction}^{air} = \frac{C_{i,fraction}^{air}}{\rho_{air}} DC_i^{ext}$ where $C_{i,fraction}^{air}$ is the activity concentration in air in Bq m^{-3} (summing the individual free, unattached and attached fractions), DC_i^{ext} is the dose coefficient for external exposure and ρ_{air} is the density of air (necessary to convert $C_{i,fraction}^{air}$ to Bq kg^{-1}, given that DC_i^{ext} has units of μGy h^{-1} Bq^{-1} kg). The total dose rate for all radionuclides is then calculated as $DR_{fraction}^{air} = \sum_{i=1}^{N} DR_{i,fraction}^{air}$. For simplicity and conservatism, an occupation factor of one is assumed.
- Dose rates from internally-incorporated radionuclide *i* in the tree are calculated as $DR_{i,tree}^{int} = C_i^{tree} DC_i^{int}$ where C_i^{tree} is the activity concentration in tree (sum of all three fraction activities divided by whole tree mass) and DC_i^{int} is the dose coefficient for internal exposure. The total dose is calculated by summation of the individual radionuclides as above.
- Similarly, surface doses are approximated as $DR_{i,tree}^{surf} = C_i^{tree\,surf} DC_i^{surf}$, where the surface dose coefficients DC_i^{surf} are those calculated for vegetation by Vives i Batlle et al. (2011). The total dose is similarly calculated by summation of the individual radionuclide components.

The model calculates doses unweighted by radiation quality. Given that ^{226}Ra, ^{222}Rn, ^{218}Po, ^{214}Pb, ^{214}Bi and ^{214}Po are, in the main, α-emitters, a radiation weighting factor RWF of 10 can be applied to the result, as per the ERICA methodology's guidance (Brown et al., 2008). The short-lived α-emitting nuclides are the predominant contributors to dose because they have high specific activity and the highest absorbed fractions.

With regards to doses to the biota inhabiting the surface of the soil, these can be calculated from the model-generated soil activity concentration in the soil layer. Given the ability of the ERICA Tool

version 2 to perform assessments on a timed series of concentrations, we see no benefit in incorporating this functionality into the model at this stage. Instead, it is easy to export a file of soil concentrations and use the ERICA Tool directly.

2.5 Model parameterisation

The model was parameterised with site-specific data from the Kempen area of Belgium, including daily readings of temperature, solar irradiation, rainfall, crop coefficient, leaf area index and sap flow. Additional generic modelling parameters for the Scots pine model tree used here were obtained from the SVAT ECOFOR model produced under EC TERRITORIES (Brown et al., 2019; Diener et al., 2017; Urso et al., 2019). With this information, the model can calculate the cycling of water, radon and its progeny between soil, trees, and atmosphere, as well as the emanation and exhalation of radon gas from soil, the formation of the aerosol of the radon progeny and its transfer to, and turnover by, the vegetation.

The parameter set used by the model are given in Table 1 below. An additional set of temperature, leaf area index, crop coefficient, irradiation and precipitation data taken at the meteorological mast of the Belgian Nuclear Research Centre in Mol, Belgium, is given in Fig. 3. For longer-duration modelling simulations (in the order of years) where sub-daily variations are not required, the model uses time-averaged minimum and maximum temperatures, leaf area index, crop coefficient, irradiation and precipitation as extracted from this dataset: 280 – 287 K, 2.17, 1.14, 115 J m^{-2} s^{-1} and 2.8×10^{-8} m s^{-1}, respectively.

Table 1: Standard parameters from the ECORADON model

Category	Subcategory	Definition	Value	Units	Uncertainty	Source
Hydrology parameters						
α		Hydraulic conductivity	11	Unitless	Medium	Kendy et al. (2003)
E		Soil emanation coefficient	0.25	Unitless	Low	UNSCEAR (1993)
η		Water dynamic viscosity	0.001	kg m^{-1} s^{-1}	Negligible	Basic
γ		Water surface tension (at 25°C)	0.0719	kg s^{-2}	Negligible	Basic
K_d	^{226}Ra	Soil-liquid distribution coefficient	8.47	m^3 kg^{-1}	High	ERICA Tool
	^{222}Rn		0	m^3 kg^{-1}	High	ERICA Tool
	^{218}Po		416	m^3 kg^{-1}	High	ERICA Tool
	^{214}Pb		372	m^3 kg^{-1}	High	ERICA Tool
	^{214}Bi		7	m^3 kg^{-1}	High	ERICA Tool
	^{214}Po		416	m^3 kg^{-1}	High	ERICA Tool
K		Radon permeability constant	1.25×10^{-11}	m^2 s^{-1}	Negligible	Basic
H_c^{sat}	Upper soil	Saturated hydraulic conductivity	2.93×10^{-5}	m s^{-1}	Med - High	Raes and Deproost (2003) empirical equation, using soil composition data
	Lower soil		3.18×10^{-7}	m s^{-1}	Med - High	Raes and Deproost (2003) equation, using soil composition data
ρ_{bulk}^{soil}	Upper soil	Soil bulk density	850	kg m^3	Negligible	Basic - using soil composition data
	Lower soil		1550	kg m^3	Negligible	Basic - using soil composition data
ρ_p^{soil}		Soil particle density (assumed	2650	kg m^3	Negligible	Basic - Baes and Sharp (1983)
h	Upper soil	Soil layer thickness	0.26	m	Negligible	By definition
	Lower soil		1.4	m	Negligible	By definition
f_c		Field capacity (sandy soil)	0.134	Unitless	Low - Med	Raes and Deproost (2003)
r_{sorp}	H_2O, ^{222}Rn	Sorption rate	0	s^{-1}	Negligible	By definition
	^{226}Ra, Rn progeny		1.736×10^{-7}	s^{-1}	Med - high	Based on K_d and soil properties
θ_{res}	All layers	Residual soil volumetric water content	0.02	Unitless	Negligible	By definition
τ		Empirical tortuosity parameter	3	Unitless	Medium	Iversen and Jørgensen (1993)
r_p		Reference soil capillary channel radius	6.5×10^{-6}	m	Low	Calculated from particle size, SSGTC (2008)
Atmospheric parameters						
ρ_{air}		Density of air at STP	1.239	kg m^{-3}	Negligible	Basic
r_{att}	H_2O, ^{226}Ra, ^{222}Rn	Attachment rate constant	0	s^{-1}	Negligible	Basic
	Rn progeny		0.02	s^{-1}	Negligible	(Porstendörfer, 1994)
r_{clust}		Clustering rate	2.3	s^{-1}	Negligible	(Porstendörfer, 1994)
C_p		Specific heat capacity of dry air	1005	J Kg^{-1} K^{-1}	Negligible	Basic
D_c^{soil}		Diffusion coefficient of radon in	1.0×10^{-6}	m^2 s^{-1}	Negligible	Basic
$D_c^{stomata}$		Diffusion coefficient of radon in	1.1×10^{-5}	m^2 s^{-1}	Low - med	Yu et al. (1993)
f_{fc}	Upper soil	Fractional field capacity	0.118	Unitless	Low – med	Calculated (Brakensiek et al. 1984; Schroeder et al. 1994)
	Lower soil		0.5	Unitless	Low - med	Calculated (Brakensiek et al. 1984; Schroeder et al. 1994)
h_{eff}		Effective mixing height	1	m	Negligible	By definition
P_A		Atmospheric pressure	1.01×10^5	Pascals	Negligible	Basic

h_{rel}		Relative humidity	0.55	Unitless	Negligible	Basic
R_{spec}		specific gas constant for dry air	287.058	J kg^{-1} K^{-1}	Negligible	Basic
v		Reference wind speed	0.001	m s^{-1}	Negligible	By definition
Vegetation parameters						
a		Allometric parameter a for pine	0.152	Kg	Low	Xiao and Ceulemans (2004)
b		Allometric parameter b for pine	2.234	Unitless	Low	Xiao and Ceulemans (2004)
r_{an}		Anaerobiosis ratio	0.9	Unitless	Low	Raes and Deproost (2003)
h_{crop}		Reference crop height value for	0.12	m	Negligible	By definition
DBH		Tree diameter at breast height	0.2897	m	Low	Van den Hoof and Thiry (2011)
r_{dec}		Decomposition rate	7.29×10^{-9}	s^{-1}	Low - med	Pausas (1997)
E		Coefficient for soil evaporation	1	Unitless	Medium	Lindroth and Perttu (1981)
LAI		Leaf area index	2	Unitless	Low	Own measurement
γ		Mean porosity of the substomatal	0.35	Unitless	Medium	Terashima et al. (2005)
h_{leaf}		Leaf thickness	2.5×10^{-4}	m	Low - Med	Pachepsky and Acock (1996)
μ_{frac}	Bark	Tree mass fractions	0.086	Unitless	Low	Own measurement
	Belowground		0.26	Unitless	Low	Own measurement
	Litter		0.01	Unitless	Low	Own measurement
	Needles		0.22	Unitless	Low	Xiao and Ceulemans (2004)
	Roots		0.191	Unitless	Low	Own measurement
	Wood		0.55	Unitless	Low	Own measurement
RD_{max}		Maximum root depth	1.4	m	Low	Vincke and Thiry (2008)
M_{sucr}		Molecular mass sucrose	0.342	kg mol^{-1}	Negligible	Basic
φ		Relative water content of tree	0.5	Unitless	Low	Pollock (1896)
μ_{phl}		Fraction of sucrose by mass	0.2	Unitless	Low	Lane (2012)
χ		Phloem drag coefficient	0.5	Unitless	Low	Nonweilwer (1975)
r_{xy}		Xylem pore radius	4×10^{-5}	m	Low - Med	Avila et al. (2023)
r_{ph}		Phloem pore radius	5×10^{-6}	m	Medium	Lisboa et al. (2019), Taiz and Zeiger (2006)
f_{abs}		Plant absorption factor	0.15	Unitless	Medium	Van den Hoof and Thiry (2012)
f_{int}		Plant interception factor	0.29	Unitless	Medium	Van den Hoof and Thiry (2012)
ρ_{plant}		Plant density	10^3	Kg m^{-3}	Negligible	Basic
ρ_{phloem}		Phloem density	1.08×10^3	Kg m^{-3}	Negligible	Lane (2012)
ρ_{tree}		Tree bullk density	700	Kg m^{-3}	Negligible	Ketterings et al. (2001)
ρ_w		Water density	10^3	Kg m^{-3}	Negligible	Basic
$\Delta\Psi_p$		Pressure differential for xylem	1.05×10^5	kg m^{-1} s^{-2}	Low	Amiji and Sandmann (2002)
$r_{\theta\varepsilon}$		Ratio of θ_{max} to porosity	1	Unitless	Negligible	By definition
σ_{st}		Stomata density	5×10^8	m^{-2}	Medium	Pachepsky and Acock (1996)
R_{st}^{min}		Stomata maximum radius	10^{-6}	m	Medium	Pachepsky and Acock (1996)
R_{st}^{max}		Stomata minimum radius	0	m	Negligible	By definition
h_T		Average tree height	35	m	Low	Rushforth (1981)
r_w		Washout rate	4.6×10^{-7}	s^{-1}	Medium	Simulated with data from Van den Hoof and Thiry (2011)
K		Tree stand surface density	0.0359	m^{-2}	Low	Van den Hoof and Thiry (2011)
Dosimetry parameters						
DCC^{ext}	^{226}Ra	Dose coefficient for external	0	µGy h^{-1}	Low	ERICA Tool
	^{222}Rn		2.3×10^{-7}	µGy h^{-1}	Low	ERICA Tool
	^{218}Po		7.0×10^{-9}	µGy h^{-1}	Low	ERICA Tool
	^{214}Pb		2.3×10^{-4}	µGy h^{-1}	Low	ERICA Tool
	^{214}Bi		1.1×10^{-3}	µGy h^{-1}	Low	ERICA Tool
	^{214}Po		4.8×10^{-8}	µGy h^{-1}	Low	ERICA Tool
DCC^{int}	^{226}Ra	Dose coefficient for internal	0	µGy h^{-1}	Low	ERICA Tool
	^{222}Rn		3.2×10^{-3}	µGy h^{-1}	Low	ERICA Tool
	^{218}Po		3.5×10^{-3}	µGy h^{-1}	Low	ERICA Tool
	^{214}Pb		7.9×10^{-5}	µGy h^{-1}	Low	ERICA Tool
	^{214}Bi		6.6×10^{-5}	µGy h^{-1}	Low	ERICA Tool
	^{214}Po		4.4×10^{-3}	µGy h^{-1}	Low	ERICA Tool
DCC^{surf}	^{226}Ra	Dose coefficient for foliar surface	0	µGy h^{-1}	Low	Vives i Batlle et al. (2011)
	^{222}Rn		0	µGy h^{-1}	Low	Vives i Batlle et al. (2011)
	^{218}Po		1.7×10^{-3}	µGy h^{-1}	Low	Vives i Batlle et al. (2011)
	^{214}Pb		8.1×10^{-5}	µGy h^{-1}	Low	Vives i Batlle et al. (2011)
	^{214}Bi		7.9×10^{-5}	µGy h^{-1}	Low	Vives i Batlle et al. (2011)
	^{214}Po		2.2×10^{-3}	µGy h^{-1}	Low	Vives i Batlle et al. (2011)
General						
S_D		Duration of 1 day in s	86400	s d^{-1}	Negligible	Basic
π		Pi	3.14159	Unitless	Negligible	Basic
g		Acceleration of gravity	9.81	m s^{-2}	Negligible	Basic
R		Ideal gas constant	8.314	J K^{-1} mol^{-1}	Negligible	Basic
i		Van 't Hoff constant	1	Unitless	Negligible	Basic
S_A		Surface area	1	m^2	Negligible	Nominal value
λ	^{226}Ra	Decay constant	1.37×10^{-11}	s^{-1}	Negligible	Basic
	^{222}Rn		2.10×10^{-6}	s^{-1}	Negligible	Basic
	^{218}Po		3.73×10^{-3}	s^{-1}	Negligible	Basic
	^{214}Pb		4.31×10^{-4}	s^{-1}	Negligible	Basic
	^{214}Bi		5.86×10^{-4}	s^{-1}	Negligible	Basic
	^{214}Po		4.23×10^3	s^{-1}	Negligible	Basic
PAEC	^{218}Po	Potential alpha energy	0.105	J m^{-3}	Negligible	Basic - Porstendörfer (1994)
	^{214}Pb		0.516	J m^{-3}	Negligible	Basic - Porstendörfer (1994)
	^{214}Bi		0.379	J m^{-3}	Negligible	Basic - Porstendörfer (1994)
	^{214}Po		6×10^{-8}	J m^{-3}	Negligible	Basic - Porstendörfer (1994)

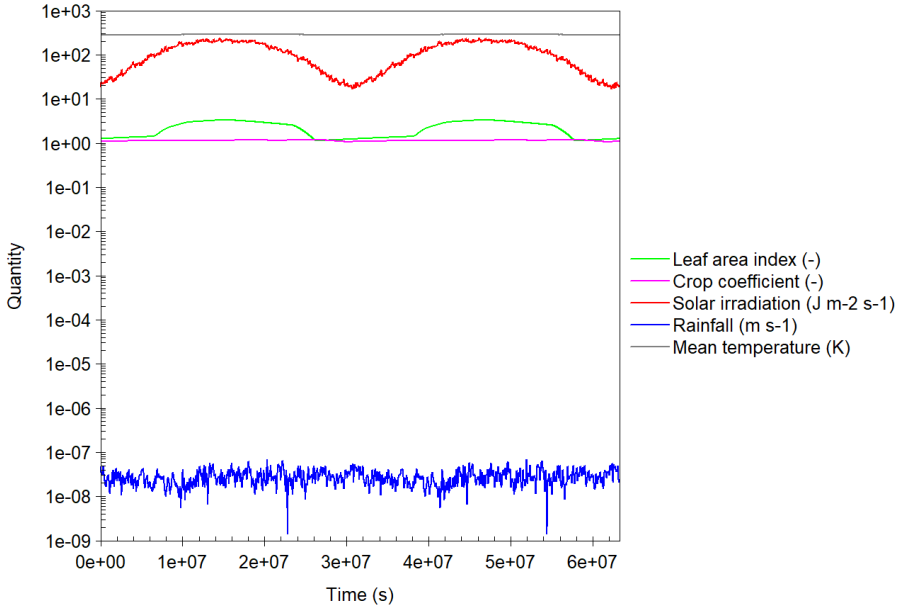

Figure 3: Time-dependent dataset of vegetation, atmospheric and solar irradiation data for the first two years of the model simulation, showing both the daily variability and the annual periodicity of the data.

Of the 109 parameters listed in Table 1, 32 (marked "basic") derive from common science knowledge. Another 10 (h for upper and lower soil, θ_{res}, r_{sorp} for water and ^{222}Rn, v, h_{eff}, h_{crop}, R_{st}^{max}, $r_{\theta\varepsilon}$ and S_A) have a value assigned by definition. These 42 parameters are qualitatively considered to have negligible uncertainty.

A group of 14 vegetation parameters were determined in the same field study area by us or by other authors (DBH, LAI, μ_{frac} for the 6 tree mass fractions, RD_{max}, h_T, ρ_{tree}, r_w, φ and K), being either dimensional/mass measurements, or calculated with empirical formulae based on soil composition (f_{fc} for upper and lower soil). These parameters are qualitatively assumed to have low uncertainty.

The next block of parameters contains 18 dose coefficients for the different radionuclides. Internal and external exposure dose coefficients (DCC^{int} and DCC^{ext}, respectively) originate from the ERICA radiological assessment tool for non-human biota (https://erica-tool.com/ERICA Tool). Surface deposition dose coefficients (DCC^{surf}) are from another source (Vives i Batlle et al., 2011). The dosimetry parameters are based on accurate physical particle tracking MonteCarlo simulations, so they are assumed to have low uncertainty.

A substantial group of 26 parameters in Table 1, either measured or equation-derived, are directly referenceable to a published source, with uncertainties qualitatively estimated to range from negligible to medium, depending on the parameter.

The 9 remaining parameters are (a) the 6 K_ds (known to have high uncertainty) and (b) the saturated hydraulic conductivities (H_c^{sat}) for upper and lower soil, together with and the soil sorption rate (r_{sorp}), assumed to have medium to high uncertainty. Uncertainty in r_{sorp} depends on K_d uncertainty because r_{sorp} is functionally linked to the desorption rate such that at equilibrium, the ratio of concentrations in unavailable and available soil fractions is equal to the K_d. Since desorption is a fast process, equilibrating soon with sorption compared with the model simulation timescales (in the order of years), the model is relatively insensitive to variability in r_{sorp}.

Our analysis suggests that only a small fraction (7%) of the model input parameters have major influence on model uncertainty, as previously noted in studies of this nature (Petropoulos et al., 2009;

Staudt et al., 2010). The K_d and the hydraulic conductivity are the principal uncertainty sources. High uncertainties in the K_d are a common feature of radioecological models (Bossew and Kirchner, 2004; Diener et al., 2017; Kirchner et al., 2009), with order of magnitude variations expected depending on experimental method, soil physico-chemical properties and sampling location. An added difficulty is that model-calculated K_ds significantly deviate from those observed in the field (Raskob et al., 2018).

A similar problem occurs with the hydraulic conductivity, complicated by its being a function of the soil's water content and physico-chemical properties (Diener et al., 2017). The hydraulic conductivity introduces significant uncertainty in the soil hydrology part of the model, as it can vary by more than one order of magnitude (Herrera et al., 2022; Sudicky, 1986). The hydraulic conductivity is usually defined according to the empirical equations (Ippisch et al., 2006; Kendy et al., 2003; van Genuchten, 1980) which are calibrated with measured values of the saturated hydraulic conductivity, leading to both experimental and modelling uncertainties.

The initial model conditions were set as follows: (a) ^{226}Ra initially present in the unavailable fraction, with activity concentration of 10^3 Bq kg^{-1}; and (b) initial volumetric water contents (θ) of 0.12 and 0.42 in soil layers 1 and 2 of the available fraction, equivalent to 0.0312 and 0.63 cubic m^3 per unit m^2 surface area, respectively. These θ are the final values of a 2-year model run with constant (averaged) meteorological conditions), i.e., we are assuming that the water balance in the soil at the beginning of the simulation is already at equilibrium.

Selectivity coefficients (SCs) for radionuclides in tree compartments, defined as the ratio between radionuclide and water transfer rates, displayed in Table 2, were obtained from the ECOFOR model created in the EC TERRITORIES project, based on empirical measurements (Brown et al., 2019; Diener et al., 2017; Gielen, 2013; Gielen et al., 2016; Urso et al., 2019).

Table 2: Selectivity coefficients (m^3 for water or Bq kg^{-1} for radionuclide)

Parameter	**Water**	**^{226}Ra**	**^{222}Rn**	**^{218}Po**	**^{214}Pb**	**^{214}Bi**	**^{214}Po**
$SC_{leaves \rightarrow air}$	1	0.00E+00	1	0.0E+00	0.0E+00	0.0E+00	0.0E+00
$SC_{leaves \rightarrow wood}$	1	1.26E-01	1	1.3E-01	1.3E-01	1.3E-01	1.3E-01
$SC_{litter \rightarrow soil}$	1	9.70E-02	1	3.2E-02	3.2E-02	3.2E-02	3.2E-02
$SC_{roots \rightarrow wood}$	1	1.80E-04	1	1.6E-04	9.8E-04	5.7E-04	1.6E-04
$SC_{soil \rightarrow root}$	1	1.58E-01	1	4.5E-02	9.6E-01	5.0E-01	4.5E-02
$SC_{wood \rightarrow leaves}$	1	3.00E-03	1	2.2E-03	4.2E-03	3.2E-03	2.2E-03
$SC_{wood \rightarrow litter}$	1	1.30E-01	1	4.1E-02	4.1E-02	4.1E-02	4.1E-02
$SC_{wood \rightarrow root}$	1	1.26E-01	1	1.3E-01	1.3E-01	1.3E-01	1.3E-01
$SC_{leaves \rightarrow litter}$	1	2.30E-01	1	3.8E-02	3.8E-02	3.8E-02	3.8E-02

Derivation of the *SC*s in these studies was conducted by an iterative numerical algorithm, backed by measurement data. The first step was to deduce initial *SC* values for ^{226}Ra, conjecturally taken to resemble the *SC*s for Mg and Ca, derived from stable element data in pine trees from the nearby Mol site (Gielen et al., 2016). For the radon progeny radionuclides, we scaled the ^{226}Ra *SC*s by the ratios of transfer factors of these elements relative to radium, obtained from a previous study (Vandenhove et al., 2009). We then used ModelMaker's numerical least-squares fitting method to vary these initial parameters iteratively until they fit with measured concentration ratios in the compartments of a purposely-sampled tree (soil, root, wood, foliage, and litter). For ^{222}Rn, a *SC* of one was assigned, signifying that radon gas does not concentrate selectively in any compartment. For ^{218}Po and ^{214}Po, we adopted the SC for ^{210}Po, the radioelement measured in the test tree. We made the same assumption for ^{214}Pb in relation to ^{210}Pb measured data.

The discrepancies between the modelled inter-compartment concentration rations and measurement data when using the optimised *SC*s ranged between 1 and 8%. The most sensitive parameters are the soil-to-root *SC*s for the various radioelements because they determine the soil-to-root solute transfer.

We verified that the calculated *SC*s resulted in the correct soil-to-whole tree transfer factors as experimentally determined, with relative differences ranging from 0.5 to 5%.

The model was implemented in the user-friendly *ModelMaker* platform (Adamatzky, 2001; Citra, 1997; Rigas, 2000). The model was executed for 2-year periods (6.32×10^7 s) using the proprietary Gear mathematical solver, designed for stiff differential equation systems. We used a set number of 7300 output points. A relative error per time step of 0.09 was decided upon after various trials. This optimises model execution speed whilst not impacting on solver accuracy. The execution times were fast, at 13 seconds. With constant (average) meteorological conditions, the model executes in 4.5 s for simulations of 25 years' duration.

3. Results and discussion

3.1 Hydrology

Model-calculated water content for the simplified 2-layer soil column over a 2-year period is given in Fig. 4. Changes in θ between the soil layers are mainly driven by the time-dependent rainfall, infiltration, and evaporation processes. The profile clearly reflects the fact that the upper part of the soil receives water inputs from the atmosphere only (i.e. precipitation) with little influence of the water table (drainage conditions). It is not possible to validate directly this calculation without soil probe moisture data taken over an extended period. However, our model calculation resembles previously measured and model-simulated contents in multi-layered forest soil from a study site in Mol (518110N, 5850E), in the centre of the Campine region of Belgium, with results ranging between 10 and 25% (Schneider et al., 2013). Our model also appears to be consistent with the volumetric water content in the top soil being generally between 10 and 20%, with fast precipitation-induced fluctuations (Vincke and Thiry, 2008).

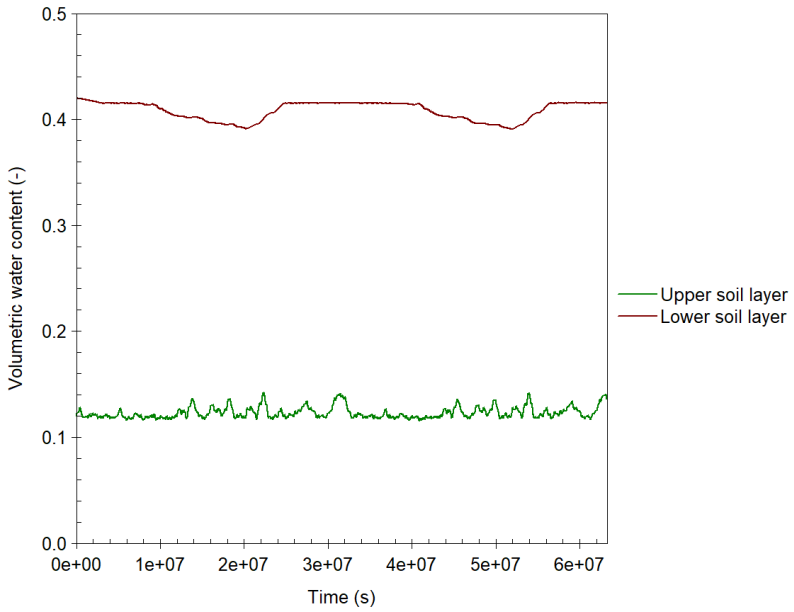

Figure 4: Model calculation of the volumetric water content (θ) in the organic surface soil layer 1 and the underlying mineral soil layer 2 over a 2-year period.

If the model starts from a dry soil column, it takes about 1 year for the hydrology to equilibrate. This is also consistent with our previous ECOFOR model, with minor differences caused by the fact that ECOFOR has a 10-layer soil model whereas our model is simplified to two soil layers.

The model-calculated potential evapotranspiration ET_0, shown in Fig. 5, exhibits annual periodicity between a minimum of 3×10^{-9} m s^{-1} and a maximum 6.2×10^{-8} m s^{-1}, super-imposed to sub-annual

fluctuations arising from the daily changes in precipitation, temperature, and solar irradiation, all of which affect directly the evaporation and transpiration fluxes. ET_0 is higher than the sum of the evaporation and transpiration fluxes because it is a theoretical value, equivalent to the maximum possible evapotranspiration. Conversely, the individual evaporation and transpiration fluxes calculated by the model are corrected by actual water availability in both tree and soil compartments.

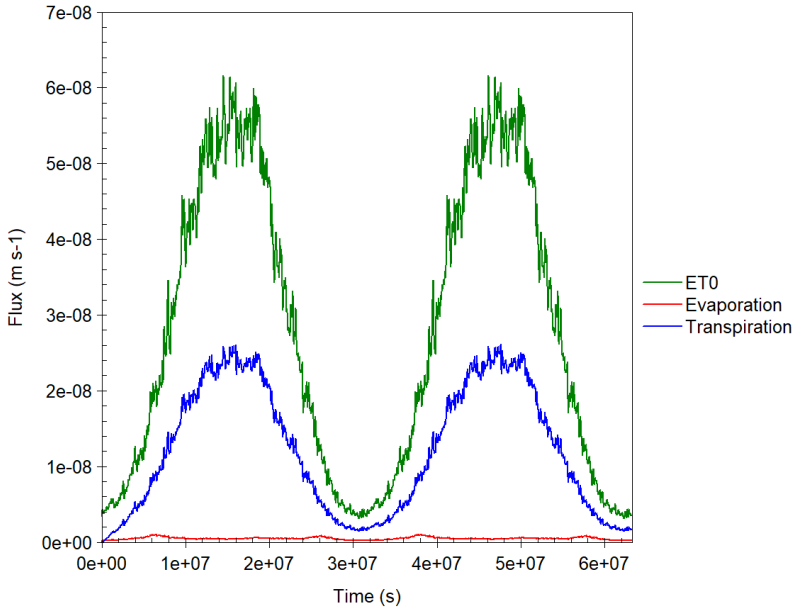

Figure 5: Representation of the reference evapotranspiration ET_0, the evaporation from soil water flux and the transpiration from plant leaves flux over a two-year period

3.2 Vegetation

The ECORADON-modelled activity concentrations of radionuclides in the two soil layers and the various tree components are given in Figs. 6 and 7, respectively.

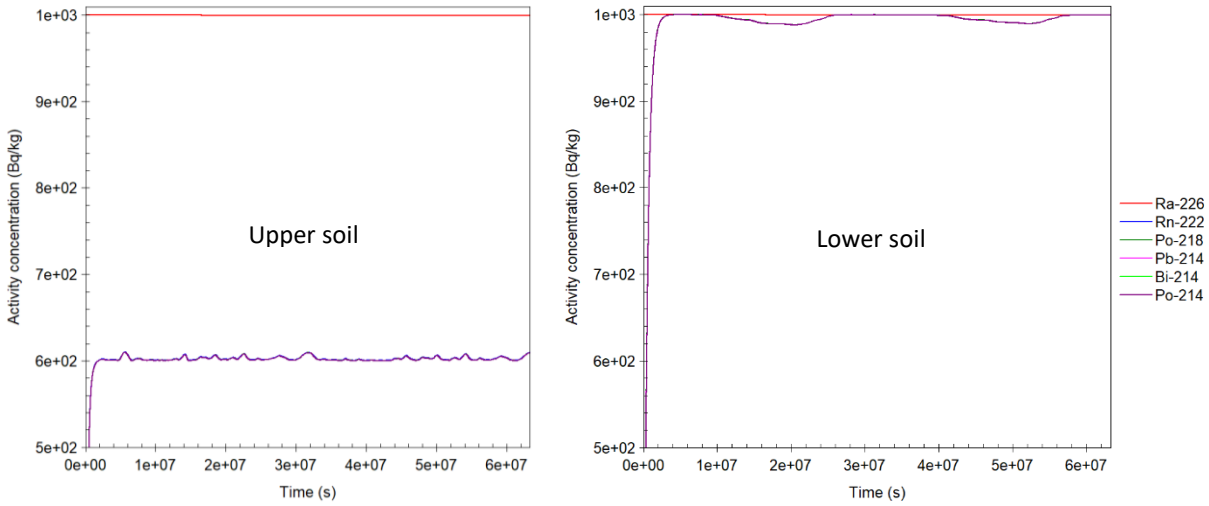

Figure 6: Model-calculated activity concentrations of radionuclides in the two soil layers.

The 2-year modelling simulation shows that as the model simulation progresses, radionuclides are gradually transferred to the available fraction and follow the soil hydrological cycle, whilst radon is exhaled to the atmosphere, forming the radon progeny aerosol, whereupon it is also taken-up by trees. From there, radionuclides can return to the soil by litterfall or root release/decomposition.

Fig. 6 shows that ^{226}Ra in soil remains constant at the initial condition of 10^3 Bq kg^{-1}, whereas ^{222}Rn overlaps with its progeny, with a rapid build-up from zero followed by daily and seasonal oscillations around 600 Bq kg^{-1} in upper soil and 10^3 Bq kg^{-1} in lower soil. The difference in behaviour between upper and lower soil is due to the action of solute fluxes between the lower soil layer and to removal by root uptake.

Fig. 7 shows activity concentrations in whole tree with and without atmospheric input of exhaled ^{222}Rn arising from the ^{226}Ra in the soil, to visualise the impact of the atmospheric processes. These simulations were conducted with the stomata radius disabled, because this smoothens the rapid daily fluctuations that would obscure the graphs.

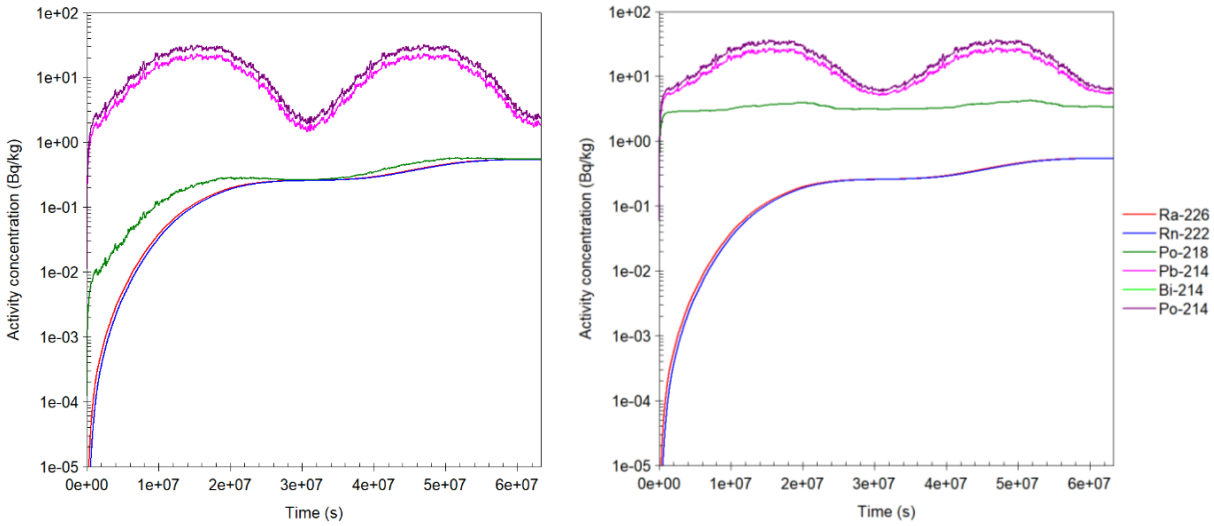

Figure 7: Model-calculated activity concentrations of radionuclides in whole tree. Left: without atmospheric input of exhaled ^{222}Rn and the progeny. Right: including atmospheric input. Note the overlap of ^{214}Bi with ^{214}Po meaning the former is not visible on the graph.

If deposition of atmospheric radon is excluded, the dominant radionuclides (^{214}Pb and ^{214}Po) reach concentrations of 1.5 and 2 Bq kg^{-1} in about 10 days, respectively. The significance of the 10-day delay is that of a model warm-up period, since the model starts computing with all radionuclide compartments set to zero (except for the soil unavailable fraction), compounded with the slow uptake of ^{226}Ra from soil via the root system. After this initial time, the model displays annual oscillations (governed by the solar, temperature and precipitation cycles) between a minimum of 1.5 Bq kg^{-1} in the winter and a maximum of 30 Bq kg^{-1} in the summer. ^{218}Po activities reach 8×10^{-3} Bq kg^{-1} after some 10 days, two orders of magnitude lower than ^{214}Po and ^{214}Pb, and a shallower annual oscillation pattern is experienced with a generally increasing trend, without attaining full periodicity in a 2-year period, due to the slow speed of the uptake process which in fact continues building-up over the lifetime of the tree. ^{226}Ra and ^{222}Rn have the lowest concentrations.

The model's output does not display approximate equilibrium between radium, radon and all the radon progeny. This is due to the multiple routes of entry of radon products into the tree. The model combines a slow uptake of ^{226}Ra from roots, leading to the formation of radon products inside the tree, with the relatively fast direct uptake of radon and its products (with no radium) from the atmosphere. Moreover, different elements have different migration rates between soil, root, and tree compartments, governed by the different K_ds and plant selectivity coefficients, meaning that physical secular equilibrium cannot be reached.

In fact, the addition of soil-exhaled radon deposition fluxes to vegetation significantly increases the uptake of ^{214}Po, ^{214}Pb and ^{218}Po by the tree, so that after some 15 days, these radionuclides have

already attained activity concentrations of 7, 6 and 3 Bq kg^{-1}. The most visually impacting result is the three-order of magnitude increase in the ^{218}Po taken-up by the tree, which undergoes a shallow ascending pattern with highly dampened annual oscillations until reaching 3.5 Bq kg^{-1} which mirror the annual variations in leaf area index. Conversely, the uptake of ^{226}Ra and its decay product ^{222}Rn remains approximately the same.

This situation can be interpreted as that the tree takes up the radon progeny principally from the atmosphere, whereas radium taken-up from soil (and the subsequent secular equilibrium concentration of radon) by the root uptake process dominates. The observable excess of atmospherically generated and plant taken-up ^{214}Po, ^{214}Pb and ^{218}Po, in comparison with the secondary progeny ingrowth mechanism by the plant after radium root uptake, is directly observable. This proves that the atmospheric interception mechanism is important, confirming our hypothesis that radon product interception is an essential mechanism when evaluating the tree uptake of ^{214}Po, ^{214}Pb and ^{218}Po and other radon products further down the decay chain. Therefore, errors of up to 120% (^{218}Po) can be incurred when this mechanism is not considered.

The dynamically-calculated soil-tree transfer factors after 2 years of exposure are given in Table 3. Given the gradual build-up of water and element concentrations in the tree over the early part of the modelling period, we decided to consider the first year as a "model warm-up period" and we focus on the second year as a better approximation to the true transfer factor. Given the annual oscillatory trend of the data, we give maximum and the minimum values corresponding to time points of 4.74×10^7 s and 6.32×10^7 s, respectively.

Table 3: Model-calculated soil-whole tree transfer factors at the time of maximum (4.74×10^7 s) and minimum (6.32×10^7 s) for the last year of 2- and 25-year simulations, respectively, including and excluding plant uptake from the atmosphere.

Run time	Deposition	Value	^{226}Ra	^{222}Rn	^{218}Po	^{214}Pb	^{214}Bi	^{214}Po
2 years	Enabled	Min	4.1E-04	5.0E-04	5.0E-03	3.4E-02	4.5E-02	4.5E-02
		Max	5.4E-04	6.7E-04	4.2E-03	6.8E-03	7.9E-03	7.9E-03
		Average	4.8E-04	5.9E-04	4.6E-03	2.0E-02	2.6E-02	2.6E-02
		Max/Min	1.3E+00	1.3E+00	8.4E-01	2.0E-01	1.7E-01	1.7E-01
	Disabled	Min	4.1E-04	5.0E-04	6.5E-04	2.8E-02	3.9E-02	3.9E-02
		Max	5.4E-04	6.7E-04	6.8E-04	2.3E-03	2.9E-03	2.9E-03
		Average	4.8E-04	5.9E-04	6.7E-04	1.5E-02	2.1E-02	2.1E-02
		Max/Min	1.3E+00	1.3E+00	1.0E+00	8.1E-02	7.5E-02	7.5E-02
25 years	Enabled	End of run	5.0E-03	6.2E-03	9.9E-03	2.3E-02	2.8E-02	2.8E-02
	Disabled	End of run	5.0E-03	6.2E-03	6.3E-03	1.8E-02	2.3E-02	2.3E-02
		Enabled/disabled	1.0E+00	1.0E+00	1.6E+00	1.3E+00	1.2E+00	1.2E+00

For ^{226}Ra and ^{222}Rn, there is no variation in uptake when the atmospheric mechanism is enabled in the model, because that there is no ^{226}Ra in the atmosphere, ^{222}Rn does not deposit onto the vegetation and, therefore, these radionuclides can only enter the plant by root uptake. For ^{218}Po, the average transfer factor considering all uptake routes is a factor of 7 higher than considering uptake from soil only. For ^{214}Pb, ^{214}Bi and ^{214}Po, the excess is by a smaller factor of 1.3. A secondary finding is that the amplitude of the seasonal oscillations of the ^{214}Pb, ^{214}Bi and ^{214}Po transfer factors becomes reduced when the atmospheric route is enabled, as shown by the Max/Min ratios in Table 3.

As mentioned previously, even a 2-year period is a relatively brief time for the tree concentrations to reach equilibrium. Prior simulations with the precursor ECOFOR model had showed the process does not attain steady state on a timescale of a few years. For this reason, we performed a long duration modelling simulation with a time integration period of 25 years, both excluding and including the atmospheric deposition process. To reduce the long execution time, we performed the simulation with averaged values of temperature, leaf area index, crop simulation, radiation, and precipitation (as discussed previously), instead of using the daily record available at our location. The results of this

model run, which allows a more realistic calculation of transfer factors for a mature tree, are given in Figure 8.

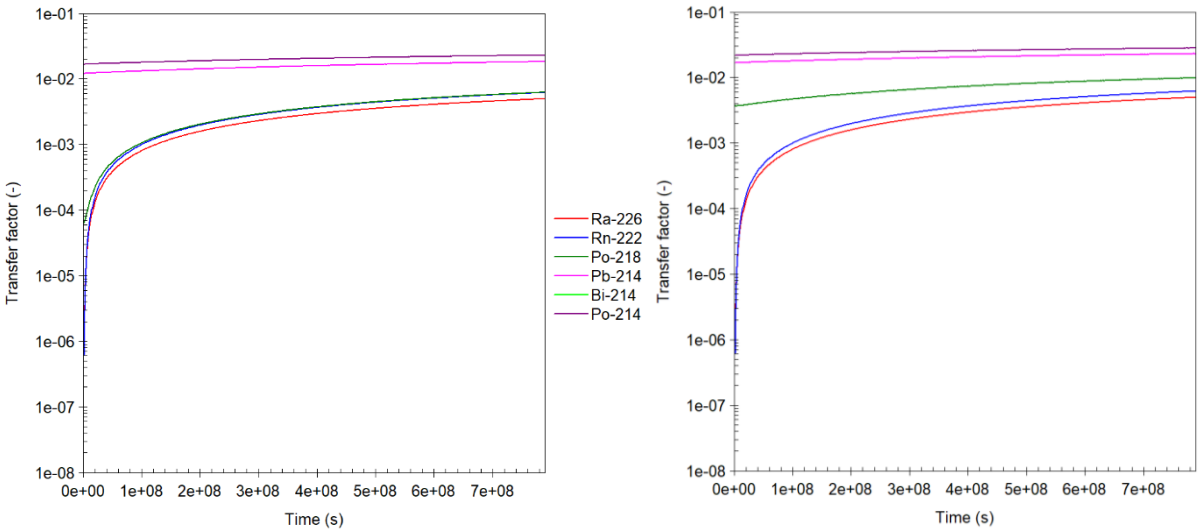

Figure 8: Model-calculated transfer factors radionuclides in whole tree (sum of roots, wood, leaf surface and leaf interior fractions). Left: simulation without atmospheric input of exhaled ^{222}Rn and the progeny. Right: simulation including atmospheric input. Note the overlap of ^{214}Bi with ^{214}Po.

The calculated transfer factors without and with atmospheric deposition component are also given in Table 3 (section for 25-year simulation). For comparison, values including atmospheric deposition are 5.0×10^{-3} (^{226}Ra), 6.2×10^{-3} (^{222}Rn), 9.9×10^{-3} (^{218}Po), 2.3×10^{-2} (^{214}Pb), and 2.8×10^{-2} (^{214}Bi and ^{214}Po). Measured transfer factors for the Kepkensberg radioecological observatory taken during the EC project TERRITORIES were $(3.1 \pm 1.8) \times 10^{-2}$ (^{226}Ra), $(3.2 \pm 1.7) \times 10^{-2}$ (^{210}Pb) and $(2.1 \pm 1.1) \times 10^{-2}$ (^{210}Po) (Brown et al., 2019). The comparativeness is limited, given the large spatial variability of the transfer factors, and the fact that the pines in the Kepkensberg site are sited on a radium-rich CaF_2 sludge heap.

A particularly important finding of this long-range calculation is that the transfer factors for ^{218}Po, ^{214}Pb, ^{214}Bi and ^{214}Po when including atmospheric deposition are 1.6, 1.3, 1.2 and 1.2 times higher, respectively, than excluding deposition, indicating the importance of this mechanism, and quantifying the error that would be committed in assessment models where this mechanism is not taken into account.

3.3 Verification of the exhalation and the radon progeny aerosol calculations

Figure 9 shows the modelled activity concentrations of ^{222}Rn and its progeny in the atmospheric aerosol, composed of free, unattached, and attached fractions. The total ^{222}Rn concentration after 2 years is 185 Bq m^{-3}. The concentration of ^{226}Ra in soil at the end of the 2-year period is 10^3 Bq kg^{-1}. This leads to a ^{222}Rn/^{226}Ra activity concentration ratio of 0.19 kg m^{-3}.

We verified the $^{222}Rn/^{226}Ra$ ratio experimentally by means of passive plastic track etching samplers in the Grote Nete Valley in the Campine region of Belgium. The experimental results give variable concentrations with an average of 122 ± 96 and 640 ± 160 Bq kg^{-1} for ^{222}Rn and ^{226}Ra, respectively (n = 8). Despite a one-order of magnitude range for both radon and radium concentrations, the $^{222}Rn/^{226}Ra$ ratio is relatively stable around a mean value of 0.24 ± 0.12 kg m^{-3}. Our ratio of 0.19 is statistically compatible with the mean value, proving that the exhalation model based on a diffusive equation is sufficiently fit for purpose.

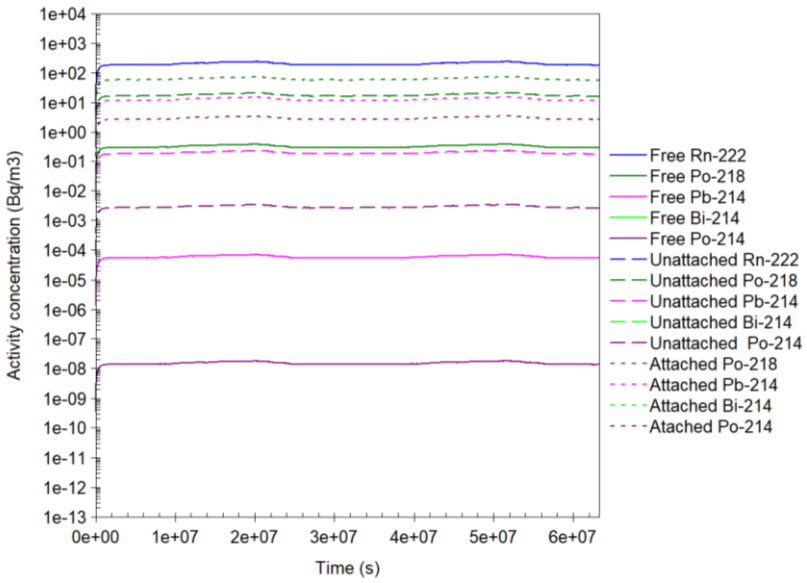

Figure 9: Activity concentrations of ^{222}Rn and its progeny in the three atmospheric aerosol components (for the case of both plant deposition and soil root uptake enabled).

In terms of aerosol composition, namely the equilibrium factor F and the fraction of the unattached progeny f_p, the model indicates F = 0.12 and f_p = 8.6% for the case in which plant deposition is not considered. With plant deposition, the results are F = 0.080 and f_p = 12.3%. This clearly confirms our hypothesis that the forest vegetation alters the make-up of the aerosol of the radon progeny by reducing the equilibrium factor and increasing the unattached progeny fraction (due to preferential removal of the unattached fraction, which has the highest deposition velocity, by the trees). In particular, (a) the equilibrium factor decreases significantly below one with plant deposition, compatible with the theoretical expectation that for higher deposition (i.e. enhanced by vegetation) F will tend to zero, and (b) the mean f_p is low, and the inverse relationship between F and f_p (James et al., 1988) is reproduced by the model.

That the model approximates well the measured ^{222}Rn concentration in air in the Belgian Nete Valley (Sweeck et al., 2024), (within a factor of < 2) indicates that the radon exhalation - aerosol formation - foliar deposition pathway is well-calculated. Radon concentration depends strongly on wind velocity.

3.4 Dose calculations

Dose rates to the trees over timescales of 2- and 25-years, unweighted by radiation quality, are shown in Figure 10. For internal exposure, ^{214}Po is the most important contributor to dose, closely followed in descending order ^{218}Po, ^{222}Rn (ingrown from ^{226}Ra taken-up by the plant), and much less significantly (two orders of magnitude below) ^{214}Pb and ^{214}Bi. This is fully consistent with results from the radon model of Vives i Batlle et al. (2011) (Vives i Batlle et al., 2011), which constitutes a point of verification for the present model.

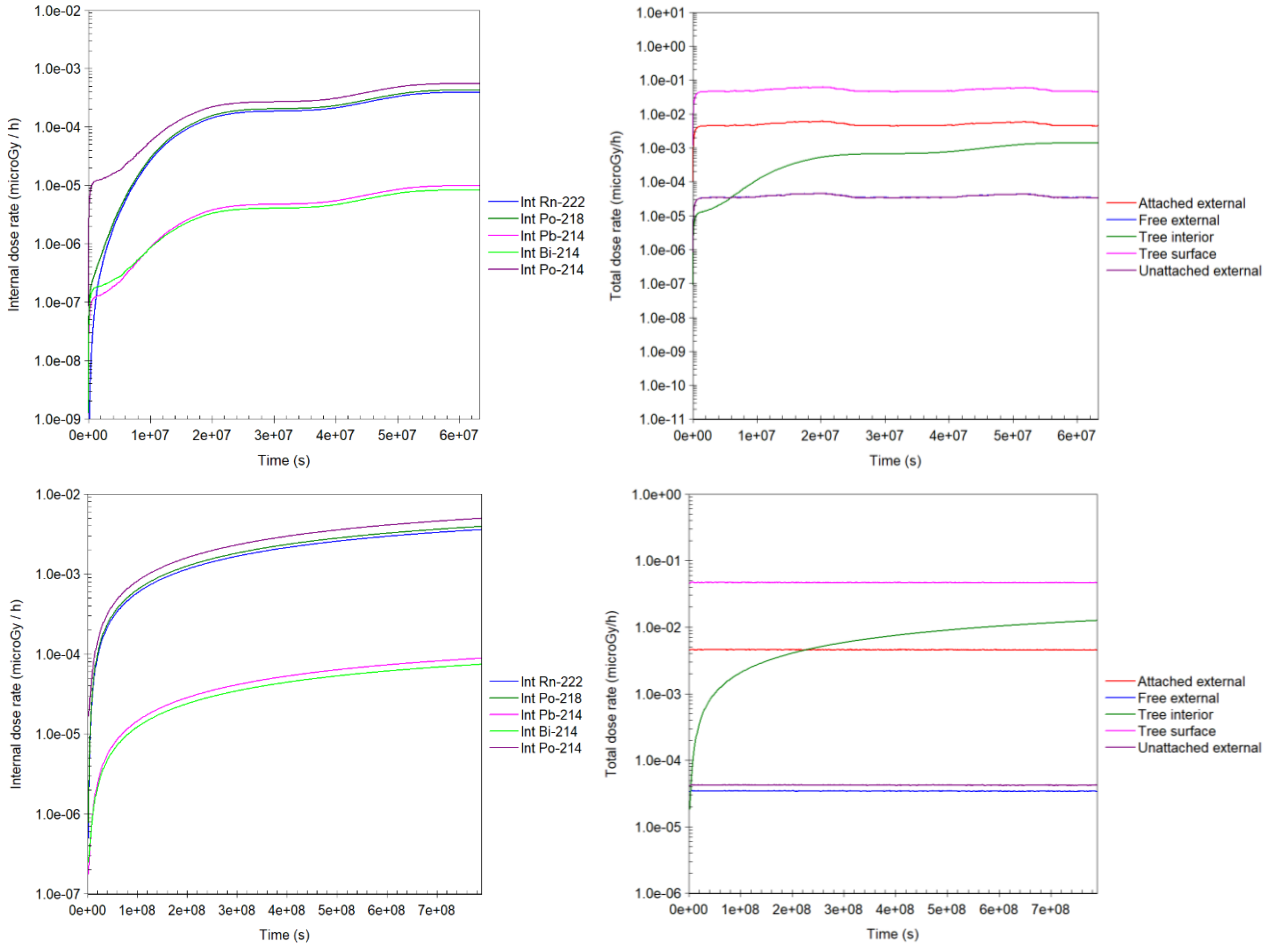

Figure 10: Unweighted dose rates to tree for the different radionuclides (left) and total dose rates (sum for all radionuclides) for internal, external, and surface dose components, over 2-year (top) and 25-year timescales (bottom). For the 2-year simulation, the external dose for free radon overlaps with the unattached component.

One of the most significant characteristics of this model is the possibility to calculate dose rates to foliage arising from the surface-deposited radon progeny (an exposure route not explicitly considered in most assessments, e.g., the ERICA Tool). This turns out to be the main dose component of the total dose rate (sum of all radionuclides), followed more than one order of magnitude below by external exposure to the attached fraction, and much further below (two orders of magnitude) the total tree internal dose and external exposures to the unattached fraction of the aerosol, respectively. In this regard, our model also gives answers consistent with our previous study on radon doses to vegetation (Vives i Batlle et al., 2011).

The internal exposure grows monotonically, surpassing the attached fraction external dose after some 17 years. This highlights the fact that the radiation dose depends on the age of the tree, since the uptake of radionuclides by the tree is a slow process. Therefore, this model allows the calculation of

(quite different) dose rates for young (2-years) and mature (25-years) trees, a fact that is also ignored in most assessment models. For internal doses, the differences between both are about one-order of magnitude, as shown in Fig. 11. For external doses, the pattern does not change.

Organism	Total Dose Rate per organism [µGy h-1]	Screening Value [µGy h-1]	Risk Quotient (expected value) [unitless]	Risk Quotient (conservative value) [unitless]
Tree	2.56E0	1.00E1	2.56E-1	7.68E-1
Amphibian	2.86E1	1.00E1	2.86E0	8.57E0
Annelid	2.92E1	1.00E1	2.92E0	8.75E0
Arthropod - detritivorous	2.91E1	1.00E1	2.91E0	8.74E0
Bird	5.12E0	1.00E1	5.12E-1	1.54E0
Flying insects	7.62E0	1.00E1	7.62E-1	2.28E0
Grasses & Herbs	2.33E1	1.00E1	2.33E0	6.98E0
Lichen & Bryophytes	9.83E1	1.00E1	9.83E0	2.95E1
Mammal - large	1.26E1	1.00E1	1.26E0	3.78E0
Mammal - small-burrowing	1.32E1	1.00E1	1.32E0	3.95E0
Mollusc - gastropod	4.08E0	1.00E1	4.08E-1	1.22E0
Reptile	2.85E1	1.00E1	2.85E0	8.55E0
Shrub	4.64E1	1.00E1	4.64E0	1.39E1

Figure 11: Assessment of dose to terrestrial biota calculated for the modelled concentrations using the ERICA tool.

The total unweighted dose rate for the tree after 25 years is 0.064 µGy h^{-1}. Using a RWF of 10 for α-emitting radionuclides, 3 for < 10 keV β-emitters (in line with ^{3}H dosimetry) and 1 for ≥ 10 keV β- and all γ-emitters results in a 10-fold increase in the total ^{222}Rn, ^{218}Po and ^{214}Po internal and surface deposition dose rates, all other doses remaining unchanged. Since the predominant contributors to dose are α-emitters, the total dose rate to the tree is approximately 0.64 µGy h^{-1}. This is well below the ERICA benchmark value of 10 µGy h^{-1}, indicating that there are no significant risks to forest vegetation in a site with soil ^{226}Ra concentrations of 10^3 Bq kg^{-1}.

An assessment with the ERICA Tool the concentration modelled (average of upper and lower soil) of 989 Bq kg^{-1} soil concentration gives a total dose rate of 2.56 µGy h^{-1}, also below 10 µGy h^{-1}. The factor of 4 difference is because ERICA has a higher in-built level of conservatism, both in terms of assuming equilibrium partitioning between vegetation and soil, and in the conservatisms involved in the ERICA calculation, particularly in terms of transfer factors and K_ds. We consider our assessment to be more realistic, and therefore reductive of conservatism.

For the concentrations in soil generated in this assessment, the ERICA Tool produces the assessment for terrestrial biota shown in Fig. 11. The screening value of 10 µGy h^{-1} is exceeded for all but Bird, Flying Insects and Gastropod. However, at the dose rates reported, no effects are predicted, based on the evidence of the FREDERICA radiation effects database (Copplestone et al., 2008).

ERICA is also able to make a radon gas assessment for breathing organisms, having implemented the method of Vives i Batlle et al. (2017). For an average radon concentration in air of 190 Bq m^{-3}, all risk quotients are below unity, the highest being for arthropod (0.38), flying insects (0.25), gastropod (0.19) and annelid (0.12), with the remainder an order of magnitude below.

It must be noted, however, that concentrations in radium-rich soils can exceed the values calculated in our case study. It has been previously noted that dose rates to burrowing mammals arising from ^{222}Rn exposure are probably an order of magnitude or more than suggested in previous assessments of natural background, which had omitted this exposure route, exceeding in some cases the screening level (Beresford et al., 2012). This suggests that, for radon, effort is required to better put the benchmarks into background context, depending on the assessment level.

4. Conclusions

A SVAT model for radon and its progeny is developed, combining a simplified soil hydrology and dynamic transfer to Scots pine trees, deriving activity concentrations in the tree (and associated soil-

vegetation transfer factors), and using exhalation rate and radon aerosol calculations. The model has a dosimetry module for dose calculations. A simple, diffusion-based, model of uptake of radon by the vegetation can represent processes that effectively remove the activity of the radon progeny deposited on plant foliage. The model can illustrate the interception of radon progeny and the reduction of the radon aerosol's equilibrium factor, as well as the further translocation of the progeny through the tree, ending in soil deposition of litterfall.

We have performed an exercise in which the model is run with and without activating the atmospheric route of entry into the tree canopy and we validated the study hypotheses. This includes our principal inference that tree uptake of the aerosol of radon progeny is a significant contribution to the total plant activity taken together with root uptake, and thus it cannot be ignored in radioecological modelling.

This model shows that several mechanisms ignored in most assessment models are, in fact, quite relevant. Such mechanisms are (a) the slow uptake of radionuclides by the tree roots, in line with observations by other modellers and for other radionuclides (Thiry et al., 2009; Van den Hoof and Thiry, 2012), meaning that concentrations never stabilise (i.e. the transfer factor is not constant) leading to different dose rates for young and mature trees, (b) the deposition of radionuclides on leaf surfaces, leading to a dominance of surface doses, (c) the difference in transfer factors for different isotopes of the same element radionuclide chain (i.e. ^{214}Po vs. ^{218}Po) and (d) the need to include radon exhalation- atmospheric deposition in assessments, without which significant errors can be made.

In this paper, we have explored the significance of uncertainties in the modelling parameters, highlighting the significance of the K_d and the hydraulic conductivity in this respect. In future work, these uncertainties should be quantified to progress this model beyond the proof-of-concept stage. This quantification ought to include single- and multi-parameter sensitivity analyses using lognormal probability density functions, confidence interval calculations or more advanced statistical methods (Bigeard et al., 2019; Staudt et al., 2010), in order to guide future radiological impact assessments.

Several parts of the model call for further development. The radon diffusion coefficient could be augmented to represent the effects of tortuosity and of atmospheric pumping in surface soil layers. Wet deposition could be included explicitly. The number of soil layers can be increased to add vertical resolution to the soil column. The model prototype could be re-cast in a programming language allowing for parallel computing, making possible to perform probabilistic calculations efficiently. Lastly, the model should be applied to different scenarios, in order to assess its transferability. Application of this model is foreseen in remediation activities planned for landfill sites with radium hotspots, where there is a need to perform radiological assessments for the trees and the forest floor biota.

5. Acknowledgement

This research was conducted within the RadoNorm project and received funding from the Euratom research and training programme 2019-20 20 under grant agreement No 900009.

6. References

Adamatzky, A., 2001. ModelMaker. Kybernetes 30, 120-125.

Amiji, M.M., Sandmann, B.J., 2002. Applied Physical Pharmacy. McGraw-Hill Professional. pp. 54–57. ISBN 0071350764.

Avila, R.T., Kane, C.N., Batz, T.A., Trabi, C., Damatta, F.M., Jansen, S., McAdam, S.A.M., 2023. The relative area of vessels in xylem correlates with stem embolism resistance within and between genera. Tree Physiology 43, 75–87.

Baes, C.F., Sharp, R.D., 1983. A proposal for estimation of soil leaching and leaching constants for use in assessments models. Journal of Environmental Quality 12, 17-28.

Bateman, H., 1910. The solution of a system of differential equations occurring in the theory of radioactive transformations. Mathematical Proceedings of the Cambridge Philosophical Society 15, 423-427.

Beresford, N., Barnett, C., Vives i Batlle, J., Potter, E.D., Ibrahimi, Z.-F., Barlow, T.S., Schieb, C., Jones, D.G., Copplestone, D., 2012. Exposure of burrowing mammals to ^{222}Rn. Science of the Total Environment 431, 252–261.

Berg, B., 2000. Litter decomposition and organic matter turnover in northern forest soils. Forest Ecology and Management 133, 13-22.

Bigeard, G., Coudert, B., Chirouze, J., Salah, E.-R., Boulet, G., Ceschia, E., Jarlan, L., 2019. Ability of a soil–vegetation–atmosphere transfer model and a two-source energy balance model to predict evapotranspiration for several crops and climate conditions. Hydrology and Earth System Sciences 23, 5033-5058.

Bossew, P., Kirchner, G., 2004. Modelling the vertical distribution of radionuclides in soil. Part 1: the convection–dispersion equation revisited. Journal of Environmental Radioactivity 73, 127-150.

Brown, J., Dvorzhak, A., Mora, J.C., Pérez-Sanchez, D., Kaasik, M., Tkaczyk, A., Hosseini, A., Iosjpe, M., Popic, J., Smith, J., Vives i Batlle, J., Almahayni, T., Vanhoudt, N., Gonze, M.-A., Calmon, P., Février, L., Hartmann, P., Steiner, M., Urso, L., Oughton, D., Christian Lind, O., Salbu, B., 2019. Guidance to select level of complexity. EC TERRITORIES Deliverable D9.61, Contract No. 662287, 171 pp. .

Brown, J.E., Alfonso, B., Avila, R., Beresford, N.A., Copplestone, D., Pröhl, G., Ulanovsky, A., 2008. The ERICA Tool. Journal of Environmental Radioactivity 99, 1371-1383.

Casadesus, J., Sauras-Yera, T., Vallejo, V.R., 2008. Predicting soil-to-plant transfer of radionuclides with a mechanistic model (BioRUR). Journal of Environmental Radioactivity 99, 864-871.

Ceulemans, R., Kowalski, A.S., Berbigier, P., Dolman, A.J., Grelle, A., Janssens, L.A., Lindroth, A., Moors, E., Rannik, U., Vesala, T., 2003. Coniferous forests (Scots and Maritime pine): carbon and water fluxes, balances, ecological and ecophysiological determinants. Ecological Studies 163, 71-97.

Chamberlain, A.C., 1991. Radioactive Aerosols. Cambridge Environmental Chemistry Series No. 3, Cambridge University Press, 255 pp.

Citra, M.J., 1997. Modelmaker 3.0 for Windows. Journal of Chemical Information and Computer Sciences 37, 1198-1200.

Copplestone, D., Hingston, J.L., Real, A., 2008. The development and purpose of the FREDERICA radiation effects database. Journal of Environmental Radioactivity 99, 1456-1463.

Copplestone, D., Johnson, M.S., Jones, S.R., 2000. Radionuclide behaviour and transport in a coniferous woodland ecosystem: The distribution of radionuclides in soil and leaf litter. Water Air and Soil Pollution 122, 389-404.

Deckmyn, G., Verbeeck, H., Op de Beeck, M., Vansteenkiste, D., Steppe, K., Ceulemans, R., 2008. ANAFORE: a stand-scale process-based forest model that includes wood tissue development and labile carbon storage in trees. Ecological Modelling 215, 345-368.

Diener, A., Hartmann, P., Urso, L., Vives i Batlle, J., Gonze, M.A., Calmon, P., Steiner, M., 2017. Approaches to modelling radioactive contaminations in forests - Overview and guidance. Journal of Environmental Radioactivity 178-179, 203-211.

El-Hussein, A., 1996. Unattached fractions, attachment and deposition rates of radon progeny in indoor air. Applied Radiation Isotopes 47, 515 - 523.

Ferrandino, F.J., Aylor, D.E., 1985. An explicit equation for deposition velocity. Boundary-Layer Meteorology 31, 197-201.

Gear, C.W., 1971. Numerical initial value problems in ordinary differential equations. Prentice-Hall, NJ.

Gielen, S., 2013. Element cycling in a Belgian pine forest. MSc Thesis, XIOS Hogeschool Limburg, Hasselt, Belgium, 153 pp.

Gielen, S., Vives i Batlle, J., Vincke, C., Van Hees, M., Vandenhove, H., 2016. Concentrations and distributions of Al, Ca, Cl, K, Mg and Mn in a Scots pine forest in Belgium. Ecological modelling 324, 1-10.

Gonze, M.-A., Renaud, P., Korsakissok, I., Kato, H., Hinton, T.G., Mourlon, C., Simon-Cornu, M., 2014. Assessment of dry and wet atmospheric deposits of radioactive aerosols: application to Fukushima radiocaesium fallout. Environmental Science & Technology 48, 11268–11276.

Herrera, P.A., Angel Marazuela, M.A., Hofmann, T., 2022. Parameter estimation and uncertainty analysis in hydrological modeling. WIREsWater 9, 1-23.

Hölttä, T., Vesala, T., Sevanto, S., Perämäki, M., Nikinmaa, E., 2006. Modeling xylem and phloem water flows in trees according to cohesion theory and Münch hypothesis. Trees – structure and function 20, 67-78.

ICRP, 2017. Dose Coefficients for Non-human Biota Environmentally Exposed to Radiation. International Commission on Radiological Protection Publication 136. Annals of the ICRP 46, 1-136.

Ippisch, O., Vogel, H.J., Bastian, P., 2006. Validity limits for the van Genuchten–Mualem model and implications for parameter estimation and numerical simulation. Advances in Water Resources 29, 1780-1789.

Iversen, N., Jørgensen, B.B., 1993. Diffusion coefficients of sulfate and methane in marine sediments: Influence of porosity. Geochimica and Cosmochimica Acta 57, 571.

James, A.C., Strong, J.C., Cliff, K.D., Stranden, E., 1988. The Significance of Equilibrium and Attachment in Radon Daughter Dosimetry. Radiation Protection Dosimetry 24, 451 - 455.

Kendy, E., Gerard-Marchant, P., Todd Walter, M., Zang, Y., Liu, C., Steenhuis, S., 2003. A soil-water balance approach to quantify groundwater recharge from irrigated cropland in the North China Plain. Hydrological Processes 17, 2011-2031.

Ketterings, Q.M., Coe, R., Noordwijk, M., Ambagau, Y., Palm, C.A., 2001. Reducing uncertainty in the use of allometric biomass equations for predicting above-ground tree biomass in mixed secondary forests. Forest Ecology and Management 146, 199-209.

Kirchner, G., Strebl, F., Bossew, P., Ehlken, S., Gerzabek, M., 2009. Vertical migration of radionuclides in undisturbed grassland soils. Journal of Environmental Radioactivity 100, 716-720.

Lane, L., 2012. Sucrose solutions, composition, viscosity, density at 20oC. Available from: http://lclane.net/text/sucrose.html [Accessed 12 December 2024].

Lerman, A., 1979. Geochemical Processes: Water and Sediment Environments. Wiley-Interscience, New York, 481 pp.

Li, K.Y., Boisvert, J.B., De Jong, R., 1999. An exponential root-water-uptake model. Canadial Journal of Soil Science 79, 333–343.

Li, K.Y., De Jong, R., Boisvert, J.B., 2001. Comparison of root-water-uptake models. In: Sustaining the Global Farm: Selected Papers from the 10th Int. Soil Conservation Organization Meeting, West Lafayette, IN, Purdue University and USDA-ARS National Soil Erosion Research Laboratory, pp. 1112–1117.

Lindroth, A., Perttu, K., 1981. Simple calculation of extinction coefficient of forest stands. Agricultural Meteorology 25, 97-110

Lisboa, L.A.M., Heinrichs, R., Figueiredo, P.A.M., 2019. Effects of Preplantation Phosphate on the Inner Morphology of Sugarcane Leaves. Journal of Plant & Soil Science 31, 1-7.

Monteith, J., Unsworth, M., 2007. Principles of Environmental Physics, Third Ed. Academic press, 418 pp.

Nonweilwer, T.R.F., 1975. Flow of biological fluids through non-ideal capillaries. Encyclopedia of Plant Physiology 1: 474-477 (New series).

Pachepsky, L.B., Acock, B., 1996. A model 2DLEAF of leaf gas exchange: development, validation, and ecological application. Ecological Modelling 93, 1 - 16.

Parkhurst, D.L., 1995. User's guide to PHREEQC- a computer program for speciation, reaction-path, advective-transport, and inverse geochemical calculations: U.S. Geological Survey Water-Resources Investigations Report 95-4227, 143 pp

Pausas, J., 1997. Litter fall and litter decomposition in Pinus sylvestris forests of the eastern Pyrenees. Journal of Vegetation Science 8, 643-650.

Perez-Sanchez, D., Thorne, M.C., Limer, L.M.C., 2012. A mathematical model for the behaviour of Se-79 in soils and plants that takes account of seasonal variations in soil hydrology. Journal of Radiological Protection 32, 11–37.

Petropoulos, G., Wooster, M.J., Carlson, T.N., Kennedy, M.C., Scholze, M., 2009. A global Bayesian sensitivity analysis of the 1d SimSphere soil–vegetation–atmospheric transfer (SVAT) model using Gaussian model emulation. Ecological Modelling 220, 2427-2440.

Pollock, J.B., 1896. On the variations in the water content of trees. University of Wisconsin-Madison, 90 pp.

Porstendörfer, J., 1994. Properties and behaviour of radon and thoron and their decay products in the air. Journal of Aerosol Science 25, 219-263.

Porstendörfer, J., Wicke, A., Schraub, A., 1978. The influence of exhalation, ventilation and deposition processes upon the concentration of radon (^{222}Rn), thoron (^{220}Rn) and their decay products in room air. Health Physics 34, 465 - 473.

Raes, D., Deproost, P., 2003. Model to assess water movement from a shallow water table to the root zone. Agricultural Water Management 62, 79-91.

Raskob, W., Almahayni, T., Beresford, N.A., 2018. Radioecology in CONFIDENCE: Dealing with uncertainties relevant for decision making. Journal of Environmental Radioactivity 192, 399-404.

Raven, P.H., Johnson, G.B., Mason, K., Losos, J., 2001. Biology. The McGraw-Hill Companies.

Richards, L.A., 1931. Capillary conducti on of liquids through porous mediums. Physics 1, 318–333.

Rigas, M.L., 2000. Software Review: Modelmaker 4.0. Risk Analysis 20, 543-544.

Rushforth, K., 1981. Pocket Guide to Trees. Simon & Schuster, 215 pp.

Saupe, S.G., 2009. Solute Transport: Phloem Structure & Function. In: Plant Physiology (Biology 327). Available from: http://employees.csbsju.edu/ssaupe/biol327/lecture/phloem.htm [Accessed: 12 December 2024].

Schmidt, V., Hamel, P., 2001. Measurements of deposition velocity of radon decay products for examination of the correlation between air activity concentration of radon and the accumulated Po-210 surface activity. Science of the Total Environment 272, 189 - 194.

Schneider, S., Jacques, D., Mallants, D., 2013. Inverse modelling with a genetic algorithm to derive hydraulic properties of a multi-layered forest soil. Australian Journal of Soil Research 51, 372-389.

Šimůnek, J., Jacques, D., Van Genuchten, M.T., Mallants, D., 2006. Multicomponent geochemical transport modeling using the HYDRUS computer software packages. Journal of the American Water Resources Association 42, 1537-1547.

SSGTC, 2008. Soil Science Glossary Terms Committee. Glossary of Soil Science Terms 2008. Madison, WI: Soil Science Society of America. ISBN 978-0-89118-851-3.

Staudt, K., E. Falge, E., R. D. Pyles, R.D., Paw U, K.T., Foken, T., 2010. Sensitivity and predictive uncertainty of the ACASA model at a spruce forest site. Biogeosciences 7, 3685–3705.

Sudicky, E., 1986. A natural gradient experiment on solute transport in a sand aquifer: Spatial variability of hydraulic conductivity and its role in the dispersion process. Water Resources Research 22, 2069–2082.

Sweeck, L., Vives i Batlle, J., Vanhoudt, N., 2024. Assessment of radiation dose to people and the wildlife inhabiting the Grote Nete catchment in Belgium. Journal of Environmental Radioactivity 273.

Tadmor, J., 1973. Deposition of ^{85}Kr and tritium released from a nuclear fuel reprocessing plant. Health Physics 24, 37 - 42.

Taiz, L., Zeiger, E., 2006. Topic 4.3 - Calculating Velocities of Water Movement in the Xylem and in Living Cells. In: Plant Physiology Online, A companion to Plant Physiology, Fifth Edition. Sinauer Associate Publishers, Sunderland, Massachusetts. .

Terashima, I., Araya, T., Miyazawa, S.I., Sone, K., Yano, S., 2005. Construction and Maintenance of the Optimal Photosynthetic Systems of the Leaf, Herbaceous Plant and Tree: an Eco-developmental Treatise. Annals of Botany 95, 507 - 519.

Thiry, Y., Colle, C., Yoschenko, V., Levchuk, S., Van Hees, M., Hurtevent, P., Kashparov, V., 2009. Impact of Scots pine (Pinus sylvestris L.) plantings on long term ^{137}Cs and ^{90}Sr recycling grom a waste burial site in the Chernobyl Red Forest. Journal of Environmental Radioactivity 100, 1062-1068.

UNSCEAR, 1993. Sources and Effects of Ionizing Radiation. United Nations Scientific Committee on the Effects of Atomic Radiation Report to the General Assembly. Annex A: Exposures from natural sources of radiation, United Nations, New York, 89 pp.

Urso, L., Ipbüker, C., Mauring, K., Ohvril, H., Vilbaste, M., Kaasik, M., Tkaczyk, A., Brown, J., Hosseini, A., Iosjpe, M., Christian Lind, O., Salbu, B., Hartmann, P., Steiner, M., Mora, J.C., Pérez-Sánchez, D., Real, A., Smith, J., Mourlon, C., Masoudi, P., Gonze, M.-A., Le Coz, M., Brimo, K., J., V.i.B., 2019. Methodology to quantify improvement - Guidance on uncertainty analysis for radioecological models. EC TERRITORIES Deliverable D9.62, Contract No. No 662287, 117 pp.

USEPA, 2004. AERMOD deposition algorithms - Science document. U.S. Environmental Protection Agency.

Van den Hoof, C., Thiry, Y., 2011. Modelling Natural Chlorine Cycling in a Coniferous Stand: Model Development and Applications. Contract report for ANDRA SCK•CEN-R-XX (in preparation), 50 pp.

Van den Hoof, C., Thiry, Y., 2012. Modellling of the natural chlorine cycling in a coniferous stand: implications for chlorine-36 behaviour in a contaminated forest environment. Journal of Environmental Radioactivity 107, 56–67.

van Genuchten, M.T., 1980. A closed-form equation for predicting the hydraulic conductivity of unsaturated soils. Soil Science Society of America Journal 44, 892–898.

Vandenhove, H., Olyslaegers, G., Sanzharova, N., Shubina, O., Reed, E., Shang, Z., Velasco, D.H., 2009. Proposal for new best estimates of the soil-to-plant transfer factor of U, Th, Ra, Pb and Po. Journal of Environmental Radioactivity 100, 721-732.

Vanhoudt, N., 2015. Sludge heap 'Kepkensberg' from Belgian phosphate industry. European Observatories for Radioecological Research – Template for the Description of Candidate Sites. EC STAR Project Report, 20 pp.

Vanhoudt, N., Van Gompel, A., Vives i Batlle, J., 2021. Distribution and behaviour of naturally occurring radionuclides within a Scots pine forest grown on a CaF2 waste deposit related to the Belgian phosphate industry. Science of the Total Environment 233, 106591.

Vincke, C., Thiry, Y., 2008. Water table is a relevant source for water uptake by a Scots pine (Pinus sylvestris L.) stand: Evidences from continuous evapotranspiration and water table monitoring. Agricultural and Forest Meteorology 148, 1419-1432.

Vives i Batlle, J., Smith, A.D., Vives-Lynch, S., Copplestone, D., Prohl, G., Strand, T., 2011. Model-derived dose rates per unit concentration of radon in air in a generic plant geometry. Radiation and Environmental Biophysics 50, 513-529.

Vives i Batlle, J., Ulanovsky, A.V., Copplestone, D., 2017. A method for assessing exposure of terrestrial wildlife to environmental radon (^{222}Rn) and thoron (^{220}Rn). Science of the Total Environment 605-606, 569-577.

Xiao, C.W., Ceulemans, R., 2004. Allometric relationships for below- and aboveground biomass of young Scots pines. Forest Ecology and Management 203, 177–186.

Yu, C., Loureiro, C., Cheng, J.-J., Jones, L.G., Wang, Y.Y., Chia, Y.P., Faillace, E., 1993. RESRAD data Collection handbook. U.S. Department of Energy, 158 pp.

Zimmermann, M.H., Ziegler, H., 1975. List of sugars and sugar alcohols in sieve-tube exudates. In: Transport in Plants, Encyclopedia of Plant Physiology, New Series Vol. 1. I. Phloem Transport, M.H. Zimmermann and J.A. Milburn, eds (New York: Springer-Verlag), pp. 245–271.